Hydrogen-Bonded Networks in Ethanol Proton Wires: IR Spectra of $(EtOH)_qH^+-L_n$ Clusters ($L = Ar/N_2$, $q \leq 4$, $n \leq 5$)

Nicola Solcà[†] and Otto Dopfer*

Institute for Physical Chemistry, University of Würzburg, Am Hubland, D-97074 Würzburg, Germany

Received: March 22, 2005; In Final Form: May 11, 2005

Isolated and microsolvated protonated ethanol clusters, $(EtOH)_qH^+-L_n$ with L = Ar and N_2, are characterized by infrared photodissociation (IRPD) spectroscopy in the 3 μm range and quantum chemical calculations. For comparison, also the spectrum of the protonated methanol dimer, $(MeOH)_2H^+$, is presented. The IRPD spectra carry the signature of H-bonded $(EtOH)_qH^+$ chain structures, in which the excess proton is either strongly localized on one or (nearly) equally shared between two EtOH molecules, corresponding to Eigen-type ion cores ($EtOH_2^+$ for $q = 1, 3$) or Zundel-type ion cores ($EtOH-H^+-HOEt$ for $q = 2, 4$), respectively. In contrast to neutral $(EtOH)_q$ clusters, no cyclic $(EtOH)_qH^+$ isomers are detected in the size range investigated ($q \leq 4$), indicative of the substantial impact of the excess proton on the properties of the H-bonded ethanol network. The acidity of the two terminal OH groups in the $(EtOH)_qH^+$ chains decreases with the length of the chain (q). Comparison between $(ROH)_qH^+$ with $R = CH_3$ and C_2H_5 shows that the acidity of the terminal O−H groups increases with the length of the aliphatic rest (R). The most stable $(EtOH)_qH^+-L_n$ clusters with $n \leq 2$ feature intermolecular H-bonds between the inert ligands and the two available terminal OH groups of the $(EtOH)_qH^+$ chain. Asymmetric microsolvation of $(EtOH)_qH^+$ with $q = 2$ and 4 promotes a switch from Zundel-type to Eigen-type cores, demonstrating that the fundamental structural motif of the $(EtOH)_qH^+$ proton wire sensitively depends on the environment. The strength of the H-bonds between L and $(EtOH)_qH^+$ is shown to provide a rather sensitive probe of the acidity of the terminal OH groups.

1. Introduction

The study of proton solvation and mobility in hydrogen-bonded (H-bonded) liquids is of fundamental importance for various physical, chemical, biological, and industrial phenomena.[1−12] To elucidate microscopic details of these processes, such as energetics and dynamics of proton transfer and transport along a proton wire, the characterization of short-lived H-bonded networks at the molecular level is required. The most direct access to such molecular details is provided by spectroscopy on the experimental side and quantum chemistry on the theoretical side.

Spectroscopic studies of H-bonded liquids are complicated by fast dynamical processes such as thermal fluctuations and quantum mechanical tunneling. The resulting large homogeneous and inhomogeneous broadening of spectral lines implies that only a limited and highly averaged description of the bulk properties can be derived.[13] In contrast, size-selected clusters isolated in the gas phase are suitable model systems to unravel molecular details of H-bonded networks present in the condensed phase. For example, a recent IR spectrum of the protonated water dimer ($H_5O_2^+$) between 600 and 1900 cm^{-1} provides the basis for the assignment of the liquid-phase spectrum and demonstrates the presence of $H_5O_2^+-$type structures in aqueous solution.[14,15] In addition, a deeper understanding of the properties of protic solvents can eventually be gained by a stepwise increase of the cluster size in order to approach the bulk limit.[16] However, so far the spectroscopic characterization of charged H-bonded cluster networks under controlled solvation conditions has been limited to a few systems, mainly because of the experimental difficulties in producing sufficient ion densities.[17]

The most sensitive techniques of (cluster) ion spectroscopy measure a consequence event induced by the absorption of one or more photons[14,17−24] rather than the attenuation of radiation due to absorption.[25,26] Recently, infrared photodissociation (IRPD) schemes have been successfully applied to several protonated solvent clusters, including $(H_2O)_qH^+$,[14,18,24,27−35] $(CH_3OH)_qH^+$,[36−38] $(H_2O)_q(CH_3OH)_pH^+$,[37,39−41] $NH_3(H_2O)_qH^+$,[42−44] and $[(CH_3)_2O]_q(H_2O)_pH^+$.[45,46] IRPD spectra of $H_5O_2^+$ are consistent with a C_2 symmetric structure (Zundel ion), with the excess proton being equally shared between both H_2O ligands.[14,18,24,28,29,33] This conclusion is supported by high-level quantum chemical calculations.[47−56] To the best of our knowledge, spectroscopic characterization of the corresponding protonated methanol dimer is still lacking. In larger protonated water and methanol clusters ($q \geq 3$), the excess proton can be strongly localized on a single solvent molecule or (nearly) equally shared between two solvent moieties, emphasizing the importance of protonated monomers (Eigen-type ions) and protonated dimers (Zundel-type ions) as fundamental building blocks in these H-bonded networks.[1−8,18,28−32,34−38,57] The preference for one or the other possibility largely depends on details of the environment, such as the cluster size, the isomer geometry, and the temperature. The recent IRPD spectra of larger $(H_2O)_qH^+$ clusters ($4 \leq q \leq 28$),[30−32,34,35] complement the earlier pioneering characterization of smaller complexes ($2 \leq q \leq 4$).[18,27−29] The most stable $(H_2O)_4H^+$ geometry is the prototypical Eigen-type ion, with a H_3O^+ core (proton donor)

* Corresponding author: E-mail: dopfer@phys-chemie.uni-wuerzburg.de. Fax: (+49) 931-888-6378. Telephone: (+49) 931-888-6377.

[†] Present address: Laboratorio Cantonale, Via Mirasole 22, CH-6500 Bellinzona, Switzerland.

10.1021/jp0514776 CCC: $30.25
Published on Web 06/25/2005

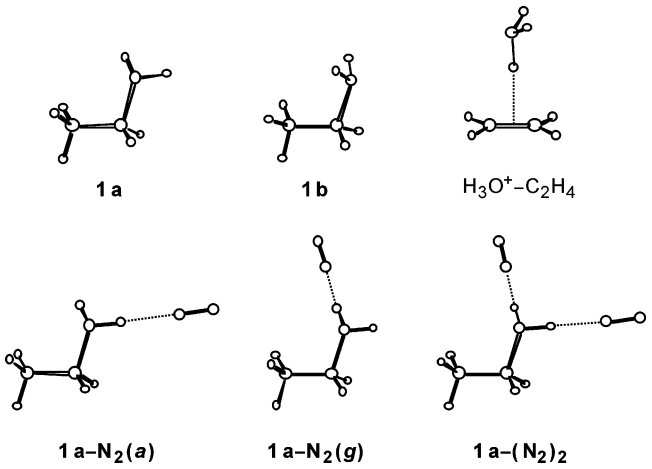

Figure 1. Calculated minimum structures (B3LYP/6-31G*) of various $C_2H_7O^+$ and $C_2H_7O^+-L_n$ isomers. The two possible rotamers of the ethyloxonium ion are labeled **1a** (gauche, C_1 symmetry) and **1b** (anti, C_s symmetry), and the ethylene−hydronium complex (C_s symmetry) is denoted as $H_3O^+-C_2H_4$. The preferred binding motif for L = Ar/N_2 to **1a/b** and $H_3O^+-C_2H_4$ is H-bonding to OH groups. As an example, possible H-bound complexes of **1a** with N_2 are shown: the anti- and gauche-bound dimers, **1a**−N_2(*a*) and **1a**−N_2(*g*), and the doubly H-bound trimer, **1a**−(N_2)$_2$.

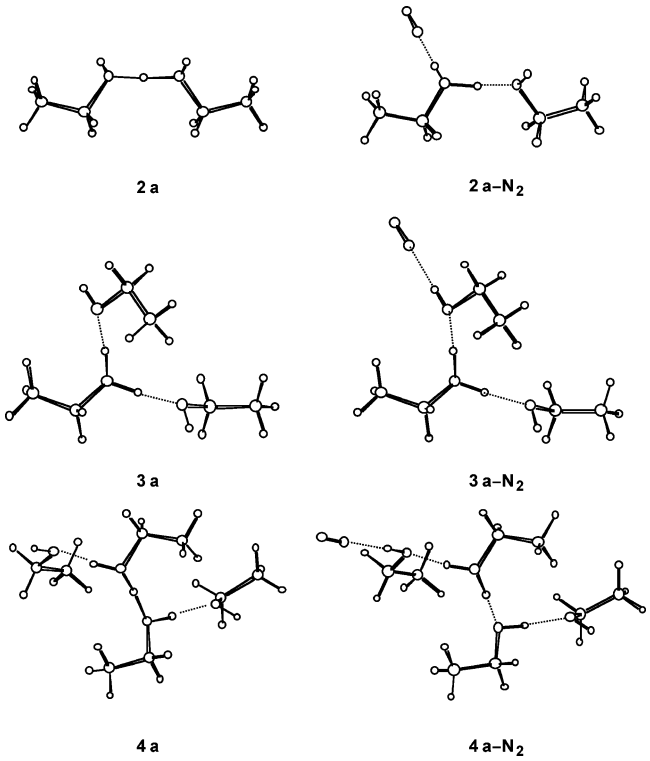

Figure 2. Calculated minimum structures (B3LYP/6-31G*) of representative H-bound isomers of $(EtOH)_qH^+$ with $q = 2-4$, **2a**−**4a**, and their H-bound $(EtOH)_qH^+-N_2$ complexes, **2a**−**4a**−N_2.

being solvated by three H_2O molecules (proton acceptors). Larger clusters display three-dimensional networks, with $q = 21$ being a very stable clathrate cage (magic number). The cluster growth of protonated methanol clusters, $(MeOH)_qH^+$, is qualitatively different from that of $(H_2O)_qH^+$, because the methyl group cannot participate in the H-bonded network. Spectroscopic data for $(MeOH)_qH^+$ have only been reported for $4 \leq q \leq 15$.[36−38] H-bonded chain structures have been postulated for $q = 2$ and 3,[36,38,58] similar to the most stable $(MeOH)_4H^+$ chain observed by IRPD spectroscopy.[36−38] The IR signature of larger aggregates show the fingerprints of linear ($q \leq 6$), cyclic ($q \geq 5$), and bicyclic ($q \geq 7$) network structures.[36,38]

The present work characterizes for the first time isolated and microsolvated protonated ethanol clusters, $(EtOH)_qH^+-L_n$, by spectroscopy. The complexes are composed of q ethanol molecules, n weakly bound inert ligands L (Ar, N_2), and a single excess proton. The spectroscopic results complement the bulk of previous mass spectrometric studies of $(EtOH)_qH^+$.[58−72] As ion−molecule association processes leading to protonated ethanol are central to models describing the synthesis of ethanol in interstellar media,[73−75] the potential energy surface (PES) of $C_2H_7O^+$ has been the subject of a number of experimental and theoretical investigations. Quantum chemical calculations predict the two classical rotamers of protonated ethanol, the ethyloxonium ion $EtOH_2^+$ ($CH_3CH_2OH_2^+$), to be the lowest energy isomers on the $C_2H_7O^+$ PES (**1a/b**, Figure 1).[59,65,76,77] Protonated dimethyl ether and various ion−dipole complexes, such as $H_3O^+-C_2H_4$ and $CH_3^+-OHCH_3$, are separated from **1a/b** by high barriers and/or lie significantly higher in energy.[59,61,63,65,76−78] Mass spectrometric studies have mainly focused on the production and reactivity of the $C_2H_7O^+$ isomers formed using different reactants, and provide information on their structure, stability, and reactivity.[59−63,65,78] Related studies involving larger $(EtOH)_qH^+$ clusters with $q > 1$ have emphasized the competition between various unimolecular decomposition reactions, such as solvent evaporation, dehydration, or loss of ethylene.[58,64−70] In general, the gas-phase reactivity of $(EtOH)_qH^+$ with neutral reagents strongly depends on the cluster size q.[69] Recently, the enthalpy barrier required for dehydration of $(EtOH)_2H^+$ was investigated in ion trapping experiments.[67,68] Moreover, the energies required to evaporate one ethanol unit from $(EtOH)_2H^+$ and $(EtOH)_3H^+$ were estimated from collision-induced dissociation experiments as $D_0 \approx 150$ and $D_0 \approx 90$ kJ/mol, respectively.[64,66] These values are consistent with early low-level AM1 calculations.[58] Surprisingly, high-level quantum chemical calculations for $(EtOH)_qH^+$ with $q > 1$ are not available.[79]

In contrast to mass spectrometry, IR spectroscopy provides a much more direct structural probe of isolated (cluster) ions. The present study extends our recent preliminary report on IRPD spectra and quantum chemical calculations of $(EtOH)_2H^+-(N_2)_n$ clusters with $n \leq 2$,[79] which showed that the excess proton is equally shared between both EtOH molecules under symmetric solvation conditions, i.e., for $n = 0$ and 2 (e.g., **2a** in Figure 2). Moreover, the properties of the O−H bonds in $(EtOH)_2H^+$ and $H_5O_2^+$ are very similar, implying that the acidity of the terminal OH groups as well as the topology of the proton-transfer potential are similar for both dimers.[79] In the present study, a large variety of smaller and larger $(EtOH)_qH^+-L_n$ clusters (L = Ar/N_2, $q = 1-4$, $n = 0-5$) are investigated to provide spectroscopic evidence for the most stable $(EtOH)_qH^+$ structures and to sensitively probe the $(EtOH)_qH^+$ PES as a function of controlled microsolvation by nonpolar ligands L via the observation of both inter- and intramolecular vibrations. The acidity of the OH groups and the related competition of intermolecular binding sites for the inert ligands L is investigated for increasing cluster size q to elucidate the impact of the additional proton on the properties of the H-bonded ethanol network. In addition, quantum chemical calculations are reported to support the interpretation of the spectroscopic results and to provide additional information on the investigated clusters not available from the experimental approach, such as dissociation energies.

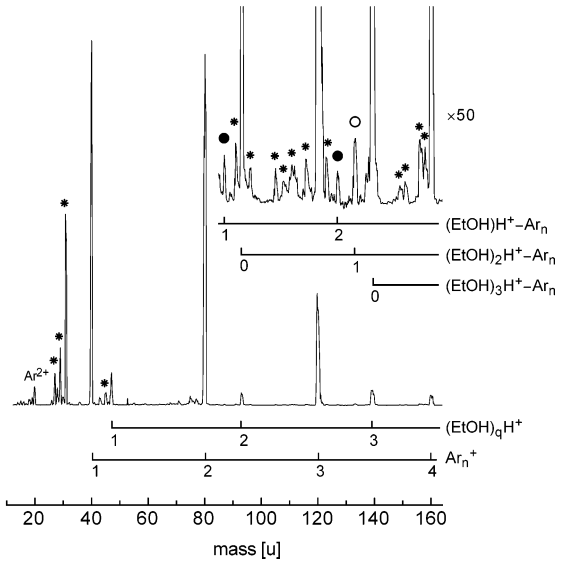

Figure 3. Mass spectrum of the electron ionization source for a coexpansion of Ar and EtOH at $p_s = 6$ bar. The most intense peaks are assigned to Ar_n^+ ($n = 1-4$), Ar^{2+}, $(EtOH)_qH^+$, and fragment ions of $EtOH_k^+$ ($k \leq 2$) and their clusters (indicated by asterisks). The vertically expanded inset (×50) demonstrates the production of weakly bound $(EtOH)_q-Ar_n$ clusters with $q = 1$ (filled circles) and $q = 2$ (open circles).

2. Experimental and Theoretical Methods

IRPD spectra of mass-selected $(EtOH)_qH^+-L_n$ clusters are recorded in a tandem quadrupole mass spectrometer (QMS1/2) coupled to an ion source and an octopole ion trap.[80] The cluster ion source combines a pulsed molecular beam expansion with electron ionization (EI). A gas mixture, obtained by passing the carrier gas (L) at a stagnation pressure of $p_s = 5-7$ bar and room temperature over an ethanol sample, expands through a pulsed nozzle into a vacuum chamber. EI of the gas mixture is accomplished by electron beams (≈100 eV) emitted from two tungsten filaments close to the nozzle orifice. Protonated ethanol is thought to be mainly generated by initial EI of EtOH followed by exothermic H atom abstraction (self-protonation):

$$EtOH + e^- \rightarrow EtOH^+ + 2e^- \quad (1a)$$

$$EtOH^+ + EtOH \rightarrow EtOH_2^+ + EtO \quad (1b)$$

Subsequent three-body association reactions yield cold $(EtOH)_qH^+-L_n$ clusters, for example via the following processes:

$$(EtOH)_{q-1}H^+-L_n + EtOH + M \rightarrow (EtOH)_qH^+-L_n + M \quad (2a)$$

$$(EtOH)_qH^+-L_{n-1} + L + M \rightarrow (EtOH)_qH^+-L_n + M \quad (2b)$$

Alternatively, $EtOH_2^+$ and its clusters may also be generated from neutral $(EtOH)_q$ precursor clusters by either fast proton-transfer reactions with Brønsted acids[81] or EI of neutral clusters followed by intracluster proton transfer and subsequent evaporative cooling.[71,81] As an example, Figure 3 shows a mass spectrum of the ion source obtained by coexpanding Ar and EtOH. As expected,[58,71,72] $EtOH_2^+$ is roughly 10 times more abundant than $EtOH^+$. Major peaks are assigned to the cluster series Ar_n^+ and $(EtOH)_qH^+$, Ar^{2+}, and fragment ions of $EtOH_k^+$ ($k \leq 2$) along with their clusters (indicated by asterisks).[64,82] The vertically expanded inset demonstrates the production of $(EtOH)_qH^+-Ar_n$ clusters.

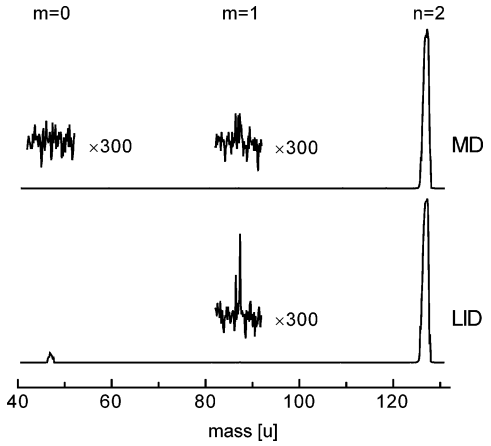

Figure 4. Mass spectra obtained by mass selecting $EtOH_2^+-Ar_2$ with QMS1 ($n = 2$) and scanning QMS2 to monitor $EtOH_2^+-Ar_m$ fragment ions ($m = 0$, 1) arising from MD (top) and additional LID at $\nu_{IR} = 3379$ cm^{-1} (bottom) in the octopole. Parts of the spectra are vertically expanded (×300) to visualize small signals.

The $(EtOH)_qH^+-L_n$ clusters of interest are mass selected from the skimmed supersonic plasma expansion by an initial quadrupole mass spectrometer (QMS1) and interact in an adjacent octopole ion guide with a tunable IR laser pulse generated by an optical parametric oscillator (OPO) laser system. Resonant vibrational excitation of the weakly bound $(EtOH)_qH^+-L_n$ clusters ($n \geq 1$) causes laser-induced dissociation (LID) of one or more of the weak intermolecular bonds:

$$(EtOH)_qH^+-L_n + \nu_{IR} \rightarrow (EtOH)_qH^+-L_m + (n-m)L \quad (3a)$$

Only this dissociation process is observed upon single-photon IR excitation for this cluster type. As expected from previous mass spectrometric studies,[64,71] for pure $(EtOH)_qH^+$ clusters (i.e., $q \geq 2$ and $n = 0$), the loss of a single EtOH molecule is observed under single-photon absorption conditions ($I_{max} = 200$ kW/cm^2):[83-85]

$$(EtOH)_qH^+ + \nu_{IR} \rightarrow (EtOH)_{q-1}H^+ + EtOH \quad (3b)$$

Although for $q \geq 2$ the loss of H_2O via a S_N2 reaction may become competitive with reaction 3b,[67,68,70,72] this channel is not considered in the present work.

The fragment ions produced are selected by a second quadrupole mass filter (QMS2) and monitored as a function of the laser frequency (ν_{IR}) to obtain the IRPD spectrum of $(EtOH)_qH^+-L_n$. As an example, Figure 4 shows a mass spectrum obtained by selecting $EtOH_2^+-Ar_2$ with QMS1 and scanning QMS2 to monitor metastable decay (MD) and LID in the octopole. MD signals corresponding to the loss of one Ar atom are hardly detected (<0.05% of $EtOH_2^+-Ar_2$), whereas the loss of both Ar ligands is below the detection limit, indicating that the clusters trapped in the octopole are cold. In contrast to MD, resonant LID of $EtOH_2^+-Ar_2$ at $\nu_{IR} = 3379$ cm^{-1} (eq 3a, section 3.2.1) causes exclusive evaporation of both Ar atoms (≈4% of $EtOH_2^+-Ar_2$). No LID signal is detected in the $EtOH_2^+-Ar$ channel. In general, the IRPD spectra discussed in section 3.2 are monitored in the dominant LID channel. Frequency calibration, accurate to better than 0.5 cm^{-1}, is accomplished by recording optoacoustic spectra of NH_3 and HDO (using the idler and signal outputs of the OPO laser, respectively) simultaneously with the IRPD spectra,[86] as well as monitoring atmospheric water absorptions along the IR laser

TABLE 1: Selected Properties of Different $(EtOH)_qH^+$ Isomers, the $H_3O^+-C_2H_4$ Complex, and EtOH Calculated at the B3LYP/6-31G* Level (Figures 1 and 2): Relative Energies (E_{rel}), Dissociation Energies (D_e), O−H Separations of the Terminal O−H Bonds (R_{OH}), Their O−H Stretch Frequencies (ν_{OH}), and IR Intensities (I_{OH})

species	E_{rel} [kJ/mol][a]	D_e [kJ/mol][b]	R_{OH} [Å]	ν_{OH} [cm^{-1}][c]	I_{OH} [km/mol]
EtOH			0.9690	3632	10
1a	0		0.9824	3560	263
			0.9825	3472	175
1b	0.4		0.9825	3558	255
			0.9825	3472	163
$H_3O^+-C_2H_4$	62.4		0.9823	3576	311
			0.9823	3488	157
			1.0884	1939	3145
2a		147.2	0.9751	3591	77
			0.9751	3589	133
3a		103.6	0.9712	3631	71
			0.9716	3621	54
4a		74.3	0.9707	3633	63
			0.9714	3618	39

[a] Corrected for zero point energy. [b] Binding energy of the most weakly bound EtOH unit. [c] Harmonic frequencies are scaled by 0.968.

path.[87] All IRPD spectra are linearly normalized for laser intensity variations measured with an InSb detector.

Density functional calculations are carried out for selected $(EtOH)_qH^+-L_n$ isomers ($q = 1-4$, $n = 0-2$, L = Ar/N_2) at the B3LYP/6-31G* level.[88] All coordinates are relaxed during the search for stationary points and the identification of minima is confirmed by vibrational analysis. To account for anharmonicity and to facilitate comparison with experimental frequencies, the harmonic frequencies are scaled by a factor of 0.968 to optimize the agreement between experimental and calculated frequencies of $EtOH_2^+-L_n$ and $(EtOH)_2H^+-L$. Intermolecular dissociation energies (D_e) of the weak bonds to N_2 and Ar are corrected for basis set superposition error.[89] For **1a/b** and $(EtOH)_{1/2}H^+-L_n$ clusters, as well as for H_3O^+ and $MeOH_2^+$, calculations are carried out also at the B3LYP/6-311G(2df,2pd) level, and the results for $(EtOH)_2H^+-(N_2)_{0-2}$ were discussed previously.[79] This level provides a more quantitative comparison with experimental data but has been too demanding to obtain results for $(EtOH)_{3/4}H^+-L_n$ with the computer resources available. If not stated otherwise, the results of the B3LYP/6-31G* calculations are discussed.

3. Results and Discussion

3.1. Theoretical Results. 3.1.1. $EtOH_2^+$. Figure 1 shows the structures calculated for different $C_2H_7O^+$ isomers relevant for the present work, and selected properties of these ions are summarized in Table 1. In agreement with previous calculations,[59,65,76,77] protonated ethanol (**1**, ethyloxonium = $EtOH_2^+$) is identified as the global minimum on the $C_2H_7O^+$ PES (Eigen-type ion). The most stable conformation of **1** corresponds to the gauche orientation of the oxygen lone pair with respect to the CH_3 group (**1a**, C_1 symmetry), whereas the anti orientation (**1b**, C_s symmetry) is a local minimum slightly higher in energy ($E_{rel} = 0.4$ kJ/mol). As reported previously,[59,65,76,77] the electrostatic π-complex $H_3O^+-C_2H_4$ (C_s symmetry) is a further local minimum on the PES ($E_{rel} = 62.4$ kJ/mol). Sophisticated calculations yield for this complex a comparable stabilization energy of $E_{rel} \approx 50$ kJ/mol with respect to **1a/b**, and the activation barriers required to interconvert **1** and $H_3O^+-C_2H_4$ are on the order of ≈84 and ≈42 kJ/mol for the forward and backward reaction, respectively.[77] Other ions and electrostatic complexes on the $C_2H_7O^+$ PES, such as protonated dimethyl ether, are well separated from **1** and $H_3O^+-C_2H_4$ by much larger isomerization barriers.[59,76,78] Consequently, the production of these species may be excluded in the present experiment.[59,61]

The properties of the O−H bonds of **1a** and **1b** relevant for the present work are rather similar ($R_{OH} \approx 0.9825 \pm 0.0001$ Å). Both rotamers feature substantially weaker, longer, and more acidic O−H bonds than neutral EtOH ($R_{OH} = 0.9690$ Å). Coupling of the two (nearly) degenerate O−H stretch local modes of **1a/b** generates a lower-frequency symmetric ($\nu_{OH,s}$) and a higher-frequency antisymmetric ($\nu_{OH,as}$) O−H stretch normal mode, with a splitting of ≈87 cm^{-1}. Their center frequency, $\nu_{OH,av} \approx 3516$ cm^{-1}, is substantially lower than ν_{OH} of EtOH (3632 cm^{-1}), confirming the destabilization of the O−H bond(s) upon protonation. The ethylene−hydronium complex features a π H-bond of H_3O^+ to the double bond of C_2H_4. As expected, the O−H donor bond is substantially longer than in bare H_3O^+ ($\Delta R_{OH} = 0.1002$ Å), whereas the two free O−H bonds contract slightly ($\Delta R_{OH} = -0.0059$ Å). These complexation-induced changes in the O−H bond lengths are directly reflected by the corresponding variations in the O−H stretch frequencies, when compared to the average O−H stretch frequency of H_3O^+ ($\nu_{OH,av} = 3466$ cm^{-1}). The bound ν_{OH} of $H_3O^+-C_2H_4$ is drastically shifted to the red ($\Delta\nu_{OH} = -1527$ cm^{-1}), and the center frequency of the free $\nu_{OH,s}$ and $\nu_{OH,as}$ modes is slightly blue-shifted ($\Delta\nu_{OH} = 66$ cm^{-1}).

3.1.2. $(EtOH)_qH^+$ Clusters ($2 \le q \le 4$). The systematic search for the preferred $(EtOH)_qH^+$ structures with $q > 1$ is complicated by the large variety of different isomers on the intermolecular PES. For example, 24 minima were found on the PES of neutral $(EtOH)_2$.[90] Significantly, the global minima on the $(EtOH)_qH^+$ PES with $2 \le q \le 4$ are clearly proton-bound structures,[58,65,67,79] similar to the related protonated methanol clusters.[36,38,58] As a detailed theoretical investigation of these structures is beyond the scope of the present work, only a single representative H-bound geometry is considered for each cluster size $2 \le q \le 4$ (**2a**−**4a**, Figure 2, Table 1). This strategy appears to be justified because, similar to the rotamers of $(EtOH)_qH^+$ with $q = 1$ (**1a/b**) and $q = 2$,[79] also the various rotamers of $q = 3$ and 4 are expected to have comparable O−H bond properties.

The excess proton in $(EtOH)_qH^+$ is either strongly localized on one or (nearly) equally shared between two EtOH molecules corresponding to clusters containing $EtOH_2^+$ (Eigen-type) or $EtOH-H^+-HOEt$ (Zundel-type) ion cores. In general, the preference for one or the other ion core depends on the number and position of EtOH molecules. In contrast to early low-level AM1 calculations, which predict an Eigen-type structure for $(EtOH)_2H^+$,[58] recent calculations at higher theoretical levels predict the Zundel-type geometry to be the most stable structural motif (Figure 2, Table 1).[79] For example, in the considered dimer **2a** with C_2 symmetry, the excess proton is exactly midway between both EtOH units ($R_{OH} = 1.2083$ Å), and also the lengths of both terminal free O−H bonds are identical ($R_{OH} = 0.9751$ Å). Alternative conformations obtained by internal rotation of the ethyl groups display very minor displacements of the central proton toward one ethanol molecule ($\Delta R = 0.0119$ Å), implying only negligible perturbations of the $O-H^+-O$ proton bridge in **2**.[79] The investigated $(EtOH)_3H^+$ structure, **3a**, corresponds to an Eigen-type core solvated by two roughly equivalent EtOH ligands. The central $EtOH_2^+$ ion features short O−H bonds ($R_{OH} = 1.0410 \pm 0.0007$ Å), whereas the intermolecular bonds with the two EtOH ligands are much longer ($R_{OH} = 1.5004 \pm 0.0002$ Å). Analysis of the R_{OH} values in the calculated

TABLE 2: Selected Properties of Different H-Bound $EtOH_2^+-L_n$ Isomers and $H_3O^+-C_2H_4-L_n$ (Figure 1) Calculated at the B3LYP/6-31G* Level: Intermolecular Dissociation Energies (D_e), H−L Distances (R_{HL}), Intermolecular Stretch Frequencies (ν_s), Complexation-Induced O−H Bond Length Changes (ΔR_{OH}), O−H Stretch Frequencies (ν_{OH}), and IR Intensities (I_{OH})

cluster	D_e [cm^{-1}]	R_{HL} [Å]	ν_s [cm^{-1}][a]	ΔR_{OH} [Å]	ν_{OH} [cm^{-1}][a]	I_{OH} [km/mol]
1a−Ar(*g*)	882	2.2882	119	−0.0008	3536	311
				0.0060	3387	583
1a−Ar(*a*)	773	2.3111	98	−0.0006	3533	282
				0.0062	3386	673
1b−Ar	837	2.2913	120	−0.0005	3531	286
				0.0062	3385	596
$H_3O^+-C_2H_4-Ar$	810	2.2933	115	−0.0004	3546	349
				0.0066	3396	595
				−0.0160	2112	3244
1a−N_2(*g*)	2676	1.8594	184	−0.0018	3539	250
				0.0161	3216	1169
1a−N_2(*a*)	2799	1.8438	168	−0.0017	3536	218
				0.0168	3202	1404
1b−N_2	2747	1.8488	187	−0.0017	3536	225
				0.0163	3207	1236
$H_3O^+-C_2H_4-N_2$	2823	1.8363	188	−0.0018	3555	271
				0.0183	3193	1248
				−0.0319	2307	3246
1a−Ar_2	825	2.2976	94	0.0048	3444	849
	747	2.3148	124	0.0053	3381	513
1b−Ar_2	780	2.2987	100	0.0052	3441	842
	780	2.2987	137	0.0052	3380	460
$H_3O^+-C_2H_4-Ar_2$	792	2.2918	94	0.0058	3445	1009
	792	2.2918	138	0.0058	3389	417
				−0.0275	2250	3213
1a−$(N_2)_2$	2499	1.8758	156	0.0122	3298	1422
	2372	1.8904	190	0.0115	3266	923
1b−$(N_2)_2$	2430	1.8853	163	0.0118	3298	1493
	2430	1.8853	200	0.0118	3266	747
$H_3O^+-C_2H_4-(N_2)_2$	2541	1.8713	165	0.0136	3277	1748
	2541	1.8713	199	0.0136	3261	669
				−0.0499	2553	2966

[a] Harmonic frequencies are scaled by 0.968.

$(EtOH)_4H^+$ isomer, **4a**, demonstrates that this conformer has a core structure intermediate between Eigen- and Zundel-type. The values of $R_{OH} \approx 1.109$ and 1.346 Å for the central $O-H^+-O$ proton bridge imply that the excess proton is displaced by 0.119 Å from the center. As the chain length increases, the terminal O−H bonds become shorter and less acidic ($R_{OH} \approx 0.9751$, 0.9714, 0.9711 Å for $q = 2-4$), in line with the sharp decrease of the binding energy of the terminal EtOH unit in the chain ($D_e = 147$, 104, 74 kJ/mol for $q = 2-4$). Along the series **1** > **2** > **3** ≈ **4**, the average O−H bond lengths (R_{OH}) decrease, the O−H stretch frequencies $\nu_{OH,av}$ increase, and the corresponding IR intensities I_{OH} decrease (Table 1). According to the calculations, the terminal EtOH units in **3a** and in **4a** are only slightly perturbed by their interior $(EtOH)_{1/2}H^+$ cores, resulting in $\nu_{OH,av}$ of **3a**/**4a** only slightly lower than ν_{OH} of neutral ethanol (≈3626 vs 3632 cm^{-1}). The correlation between the terminal O−H bond lengths and stretch frequencies demonstrates that IR spectroscopy in the O−H stretch range is a suitable tool to probe the size-dependent acidity of the free O−H bonds in $(EtOH)_qH^+$ proton wires.

3.1.3. $(EtOH)_qH^+-L_n$ Clusters (L = Ar, N_2). According to the experimental data discussed in section 3.2, the most stable $(EtOH)_qH^+-L_{1/2}$ clusters, denoted **1**−**4**−$L_{1/2}$, feature nearly linear intermolecular H-bonds between the terminal OH groups of **1**−**4** and the nonpolar ligands L = Ar/N_2 (Figures 1 and 2). The preference for this binding motif is not surprising, and has been reported for related cation−L_n systems.[17,81,91−114] Intermolecular H-bonds in cation−Ar complexes are mainly stabilized by charge-induced dipole interactions.[17,110,114] The corresponding intermolecular cation−N_2 bonds are additionally stabilized by charge−quadrupole interaction, which aligns the N_2 molecule toward the positive charge of the cation.[17,114] The weak intermolecular H-bonds to Ar and N_2 induce significant changes in the O−H bond properties of **1**−**4**, and relevant intra- and intermolecular parameters of selected **1**−**4**−L_n clusters are summarized in Tables 2 and 3. The acidity order of the free O−H bonds in bare **1**−**4** discussed in section 3.1.2 correlates with the strength of the intermolecular H−L bond(s) in

TABLE 3: Selected Properties of Different H-Bound $(EtOH)_qH^+-L_n$ Isomers (Figure 2) Calculated at the B3LYP/6-31G* Level: Dissociation Energies (D_e), H−L Distances (R_{HL}), Intermolecular Stretch Frequencies (ν_s), Complexation-Induced O−H Bond Length Changes (ΔR_{OH}), O−H Stretch Frequencies (ν_{OH}), and IR Intensities (I_{OH})[a]

cluster	D_e [cm^{-1}]	R_{HL} [Å]	ν_s [cm^{-1}][b]	ΔR_{OH} [Å]	ν_{OH} [cm^{-1}][b]	I_{OH} [km/mol]
2a−Ar	367	2.4877	99	−0.0006	3597	95
				0.0030	3546	304
2a−Ar_2	331	2.5048	78	0.0018	3567	245
	331	2.5048	103	0.0018	3554	303
2a−N_2	1648	1.9986	157	−0.0016	3606	81
				0.0090	3448	680
2a−$(N_2)_2$	1382	2.0479	140	0.0051	3511	421
	1382	2.0479	146	0.0051	3501	667
3a−N_2	1028	2.1190	148	−0.0001	3620	51
				0.0035	3584	398
3a−$(N_2)_2$	999	2.1307	135	0.0026	3589	187
	926	2.1593	147	0.0033	3588	488
4a−N_2	920	2.1484	128	−0.0002	3619	38
				0.0028	3600	352
4a−$(N_2)_2$	900	2.1533	123	0.0026	3609	219
	727	2.2128	128	0.0013	3603	347

[a] Only the two terminal OH groups of $(EtOH)_qH^+$ are considered. [b] Harmonic frequencies are scaled by 0.968.

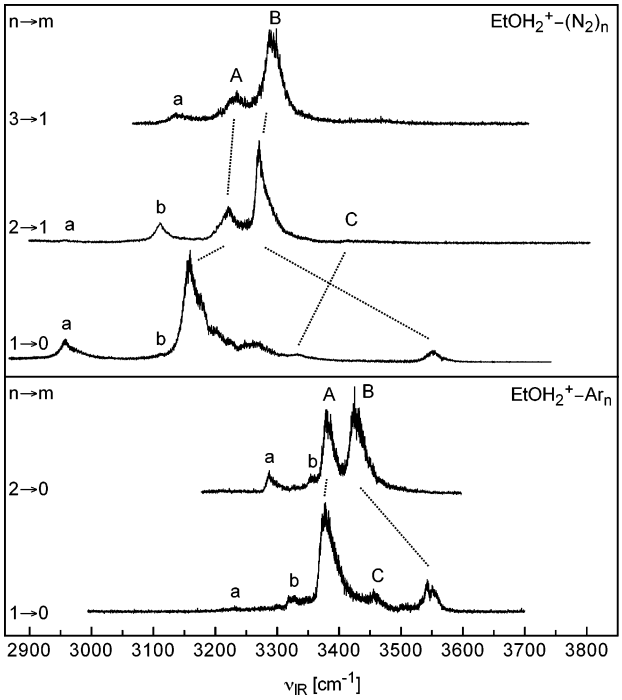

Figure 5. IRPD spectra of $EtOH_2^+-L_n$ recorded in the $EtOH_2^+-L_m$ fragment channel (L = Ar/N_2), indicated as $n \rightarrow m$ (eq 3a). The observed transitions are assigned in Table 4. Corresponding transitions are connected by dotted lines.

1−**4**−L_n. This trend is demonstrated by the increasing intermolecular separations (R_{HL}) and the decreasing dissociation energies (D_e) along the series **1**−$L_n \rightarrow$ **2**−$L_n \rightarrow$ **3**−$L_n \rightarrow$ **4**−L_n for both $n = 1$ and 2, respectively. As already discussed in ref 79, asymmetric (micro)solvation may induce a switch from Zundel-type to Eigen-type ion cores. For example, complexation of **2** with a single Ar/N_2 ligand causes such a switch, resulting in the Eigen-type structure **2**−L (e.g., **2a**−N_2 in Figure 2). In contrast, attachment of a second ligand to the free OH group of **2**−L restores a symmetric solvation environment, leading again to Zundel-type structures for **2**−L_2.[79] A related solvation-dependent geometry change of the internal $(EtOH)_2H^+$ core is also predicted for **4**: conformer **4a**, which features a central $(EtOH)_2H^+$ core intermediate between Eigen- and Zundel-type structures, switches to a clear $EtOH_2^+$−type structure when forming **4a**−N_2 (Figure 2). In general, formation of the weak intermolecular bonds between **1**−**4** and L destabilizes the terminal intramolecular O−H bond(s) involved in H-bonding ($\Delta R_{OH} > 0$), induces red shifts for the corresponding ν_{OH} modes ($\Delta\nu_{OH} < 0$) and an enhancement of their IR intensities (Tables 1−3). Again, the magnitude of these trends decreases along the series **1**−$L_n \rightarrow$ **2**−$L_n \rightarrow$ **3**−$L_n \rightarrow$ **4**−L_n for both $n = 1$ and 2. Finally, all effects described are larger for L = N_2 than for L = Ar, because of the stronger interaction in the former complexes arising from the larger polarizability and the additional quadrupole moment of N_2 ($\alpha_{||} = 2.38$ Å^3, $\Theta = -5.00$ C m^2) as compared to Ar ($\alpha_{||} = 1.64$ Å^3).[17,114]

3.2. Experimental Results. 3.2.1. $EtOH_2^+-L_n$ Clusters (L = Ar, N_2). Figure 5 compares the IRPD spectra of $EtOH_2^+-L_n$ recorded in the $EtOH_2^+-L_m$ fragment channel, indicated as $n \rightarrow m$ (eq 3a). The positions, widths, and assignments of the transitions observed are listed in Table 4. The spectra are dominated by two bands, denoted A and B. On the basis of their positions, profiles, and complexation-induced band shifts, as well as the comparison with the quantum chemical calculations, they are attributed to the two O−H stretch fundamentals of **1**−L_n. In the dimer spectra, A and B correspond to the bound and free O−H stretch modes of H-bound **1**−L, $\nu_{OH,b}$ and $\nu_{OH,f}$, respectively. The blue shaded band profile of A, with a sharp P branch head and sequence hot bands involving intermolecular modes to higher frequency from the band origin of the fundamental, is characteristic for proton donor stretch vibrations.[97,100,107−109] This shape arises from the stronger and shorter intermolecular H−L bond in the $\upsilon_{OH,b} = 1$ excited state. In contrast, the $\nu_{OH,f}$ band (B) is rather symmetric, consistent with the small influence of this vibrational excitation on the intermolecular interaction.[100,107−109] Both the $\nu_{OH,b}$ and the $\nu_{OH,f}$ frequencies calculated for the various isomers of **1**−Ar (≈3386 and ≈3533 cm^{-1} for **1a/b**−Ar) compare favorably with the corresponding experimental frequencies of A and B, 3377 and 3547 cm^{-1}. Similar agreement is observed between $\nu_{OH,b}$ and $\nu_{OH,f}$ frequencies calculated for the **1**−N_2 isomers (≈3208 and ≈3537 cm^{-1} for **1a/b**−N_2) and the corresponding measured

TABLE 4: Band Maxima, Widths (Fwhm, in Parentheses), and Assignments of Vibrational Transitions Observed in the IRPD Spectra of $(EtOH)_qH^+-L_n$ (Figures 5−7)

L	q	n	band	position [cm^{-1}]	mode	cluster
Ar	1	1	B	3547 (22)	$\nu_{OH,f}$	**1**−Ar
		1	C	3458 (15)	$\nu_{OH}+\nu_s$	**1**−Ar
		1	A	3377 (25)	$\nu_{OH,b}$	**1**−Ar
		1	b	3325 (16)	*a*	*a*
		1	a	3228 (18)	*a*	*a*
		2	B	3424 (22)	$\nu_{OH,as}$	**1**−Ar_2
		2	A	3379 (16)	$\nu_{OH,s}$	**1**−Ar_2
		2	b	3355 (14)	*a*	*a*
		2	a	3287 (14)	*a*	*a*
N_2	1	1	B	3551 (23)	$\nu_{OH,f}$	**1**−N_2
		1	C	3333 (20)	$\nu_{OH}+\nu_s$	**1**−N_2
		1	A	3158 (28)	$\nu_{OH,b}$	**1**−N_2
		1	b	3112 (16)	*a*	*a*
		1	a	2956 (23)	*a*	*a*
		2	C	3414 (28)	$\nu_{OH}+\nu_s$	**1**−$(N_2)_2$
		2	B	3270 (15)	$\nu_{OH,as}$	**1**−$(N_2)_2$
		2	A	3221 (20)	$\nu_{OH,s}$	**1**−$(N_2)_2$
		2	b	3110 (16)	*a*	*a*
		2	a	2957 (18)	*a*	*a*
		3	B	3289 (24)	$\nu_{OH,as}$	**1**−$(N_2)_3$
		3	A	3232 (24)	$\nu_{OH,s}$	**1**−$(N_2)_3$
		3	a	3136 (24)	*a*	*a*
−	2	0	D	3625 (94)	ν_{OH}	**2**
Ar	2	1	B	3625 (10)	$\nu_{OH,f}$	**2**−Ar
		1	A	3571 (20)	$\nu_{OH,b}$	**2**−Ar
N_2	2	1	B	3633 (20)	$\nu_{OH,f}$	**2**−N_2
		1	A	3490 (24)	$\nu_{OH,b}$	**2**−N_2
		2	D	3524 (20)	ν_{OH}	**2**−$(N_2)_2$
		3	D	3532 (28)	ν_{OH}	**2**−$(N_2)_3$
		4	D	3539 (16)	ν_{OH}	**2**−$(N_2)_4$
		5	D	3544 (24)	ν_{OH}	**2**−$(N_2)_5$
−	3	0	D	3639 (34)	ν_{OH}	**3**
N_2	3	1	B	3652 (18)	$\nu_{OH,f}$	**3**−N_2
		1	A	3609 (15)	$\nu_{OH,b}$	**3**−N_2
		2	D	3613 (18)	ν_{OH}	**3**−$(N_2)_2$
−	4	0	D	3649 (30)	ν_{OH}	**4**
N_2	4	1	B	3662 (8)	$\nu_{OH,f}$	**4**−N_2[b]
		1	A	3632 (14)	$\nu_{OH,b}$	**4**−N_2
		1	E	3604 (8)	$\nu_{OH,b}$	**3**−N_2−EtOH[c]
		1	F	3360 (140)	$\nu_{OH,b}$[d]	$(EtOH)_4H^+-N_2$[d]
		2	B	3658 (8)	$\nu_{OH,f}$	$(EtOH)_4H^+-(N_2)_2$[e]
		2	A	3634 (12)	ν_{OH}	**4**−$(N_2)_2$
		2	E	3603 (6)	$\nu_{OH,b}$	**3**−$(N_2)_2$−EtOH[c]

[a] Probably hot bands of **1**−L_n. [b] Contributions of less stable $(EtOH)_4H^+-(N_2)_n$ isomers cannot be excluded. [c] Tentative assignment. [d] The detailed vibrational and isomer assignment is ambiguous (see text). [e] Less stable $(EtOH)_4H^+-(N_2)_2$ isomer with at least one free OH group.

frequencies (3158 and 3551 cm^{-1}). Moreover, also the calculated and experimental IR intensity ratios of $\nu_{OH,f}$ and $\nu_{OH,b}$ show qualitative agreement for both the Ar and the N_2 complexes.

Further solvation of the H-bound **1**−L dimer by a second ligand leads to doubly H-bound structures **1**−L_2 (Figure 1), featuring two (nearly) equivalent intermolecular H−L bonds. The $\nu_{OH,f}$ mode of **1**−L transforms into the bound $\nu_{OH,as}$ vibration of **1**−L_2 and causes a pronounced complexation-induced red shift of band B. In contrast, $\nu_{OH,b}$ of **1**−L transforms into the bound $\nu_{OH,s}$ mode and, as a consequence, band A experiences a small blue shift.[81,108−110] The experimental shifts for A and B, +2 and −123 cm^{-1} (Ar) and +63 and −281 cm^{-1} (N_2), compare favorably with the corresponding calculated shifts of ≈+5 and ≈−90 cm^{-1} (Ar) and ≈+58 and ≈−240 cm^{-1} (N_2). As both OH donor groups of **1** in doubly H-bonded **1**−L_2 are solvated, the corresponding O−H stretch transitions display blue shaded profiles. Moreover, the lack of IR signals above 3500 cm^{-1} in the $EtOH_2^+$−L_2 spectra confirms that H-bonding to the OH donor groups is the preferred Ar/N_2 recognition motif of **1**, whereas other binding sites are significantly less stable.

The binding sites for further ligands in larger **1**−L_n clusters ($n > 2$) are less certain and include H-bonding to C−H donors of the ethyl group or further solvation of the oxonium group. In general, these ligands are expected to cause only minor perturbations of the O−H bonds of the doubly H-bonded **1**−L_2 core. Indeed, both O−H stretch vibrations of **1**−$(N_2)_3$ are easily identified in the $EtOH_2^+$−$(N_2)_3$ spectrum at 3232 (A, $\nu_{OH,s}$) and 3289 (B, $\nu_{OH,as}$) cm^{-1} and display only minor blue shifts of +11 and +19 cm^{-1} from the corresponding **1**−$(N_2)_2$ transitions, respectively. Hence, the third N_2 ligand has a small destabilizing effect on the two intermolecular H−N bonds of **1**−$(N_2)_2$, which in turn strengthens both intramolecular O−H bonds. Such noncooperative three-body effects arise from nonadditive induction interactions which are typical for ion solvation by nonpolar ligands.[17,81,91,93,96,98,100,101,103−105,108,109,111−114]

In addition to both O−H stretch fundamentals of **1**−L_n (A and B), other weaker features are present in the $EtOH_2^+$−L_n spectra. Bands C are assigned to combination bands of bound O−H stretch vibrations with their corresponding intermolecular H−L stretch modes (ν_s). Similar combination bands were previously observed for related H-bound cation−L_n clusters.[17,91,97,98,100,107−109] For the $EtOH_2^+$−L dimers, $\nu_{OH,b}+\nu_s$ at 3458 (Ar) and 3333 (N_2) cm^{-1} give rise to ν_s = 81 and 175 cm^{-1} for **1**−Ar and **1**−N_2 in the $\upsilon_{OH,b} = 1$ state, similar to the calculated ν_s fundamentals of ≈112 (Ar) and ≈180 (N_2) cm^{-1}, respectively (Table 2). Band C in the $EtOH_2^+$−$(N_2)_2$ spectrum occurs 193 and 144 cm^{-1} to the blue of $\nu_{OH,s}$ (A) and $\nu_{OH,as}$ (B) and is attributed to a combination band of $\nu_{OH,s}$ and/or $\nu_{OH,as}$ with one of the two possible intermolecular stretch modes ($\nu_{s,s}$ and $\nu_{s,as}$). The calculations predict $\nu_{s,s}$ and $\nu_{s,as}$ as ≈160 and ≈195 cm^{-1}, leading to possible assignments for C as $\nu_{OH,s}+\nu_{s,as}$ and/or $\nu_{OH,as}+\nu_{s,s}$ of **1**−$(N_2)_2$, or less specifically $\nu_{OH}+\nu_s$ (Table 4). The decreasing IR intensity of the $\nu_{OH}+\nu_s$ bands for increasing cluster size prevents detection of these transitions in the $EtOH_2^+$−Ar_2 and $EtOH_2^+$−$(N_2)_3$ spectra.[108,109]

The assignment of the remaining weak bands in the $EtOH_2^+$−L_n spectra (denoted a/b) is not straightforward, and species other than $EtOH_2^+$−L_n cannot be completely ruled out as carriers of these bands. As described in section 3.1.1, the H_3O^+−C_2H_4 complex is a local minimum on the $C_2H_7O^+$ PES, and is separated from the global minimum **1** by an isomerization barrier of ≈42 kJ/mol.[77] Consequently, bands a/b may originate from O−H stretch modes of H_3O^+−C_2H_4−L_n complexes. Such clusters may be formed in the ion source, for example, by isomerization of internally excited **1** toward H_3O^+−C_2H_4 followed by three-body associative cooling reactions involving L. The calculated ν_{OH} frequencies of H_3O^+−C_2H_4−L_n, however, compare unfavorably with the experimental bands a/b (Table 2, Figure 5). As discussed in section 3.1.1, other ions and electrostatic complexes on the $C_2H_7O^+$ PES are not likely to be produced in the present experiment. Further possible carriers of bands a/b in the $EtOH_2^+$−$(N_2)_n$ spectra are contaminations of the form H_3O^+−$(N_2)_{n+1}$, which have the same mass. Indeed, the mass spectrum in Figure 3 shows a small H_3O^+ signal (m = 19 u) arising from small water impurities in the gas inlet system. On the other hand, the bands a/b also appear in the corresponding $EtOH_2^+$−Ar_n spectra, which cannot be contaminated by such clusters. Most likely, bands a/b arise from hot bands of $EtOH_2^+$−L_n, originating from intermolecular vibrations and terminating at O−H stretch fundamentals.[94]

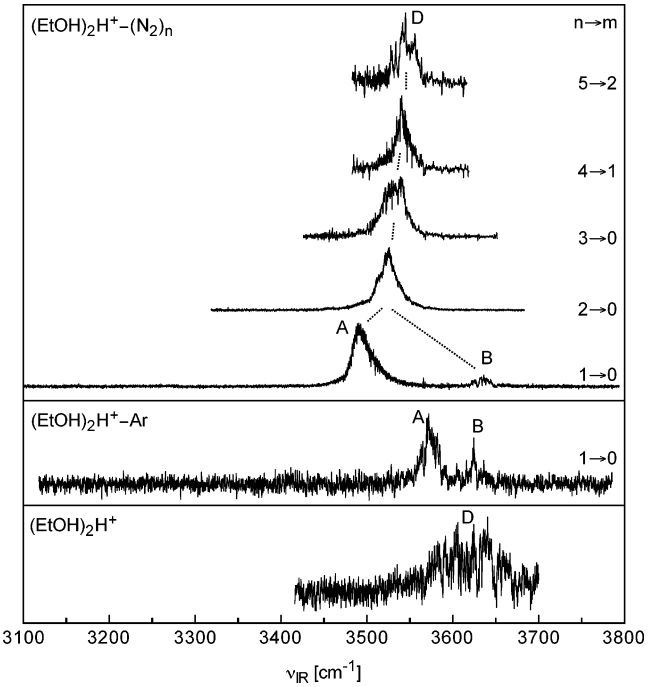

Figure 6. IRPD spectra of $(EtOH)_2H^+$−L_n recorded in the $(EtOH)_2H^+$−L_m fragment channel (L = Ar/N_2), indicated as $n \rightarrow m$ (eq 3a). The $(EtOH)_2H^+$ spectrum is obtained in the EtOH loss channel (eq 3b). The observed transitions are assigned in Table 4. Corresponding transitions are connected by dotted lines.

3.2.2. $(EtOH)_2H^+$−L_n Clusters (L = Ar, N_2). Figure 6 compares the IRPD spectra of $(EtOH)_2H^+$−L_n with L = Ar ($n \leq 1$) and N_2 ($n \leq 5$). The bare $(EtOH)_2H^+$ spectrum is monitored in the EtOH loss channel (eq 3b), whereas the $(EtOH)_2H^+$−L_n spectra are obtained in the $n \rightarrow m$ fragment channels (eq 3a). The positions, widths, and assignments of the transitions observed are listed in Table 4. The $(EtOH)_2H^+$−$(N_2)_n$ spectra with n = 0−2 have already been discussed in ref 79. Band D at 3625 cm^{-1} in the $(EtOH)_2H^+$ spectrum arises from the unresolved $\nu_{OH,s}$ and $\nu_{OH,as}$ modes of Zundel-type $(EtOH)_2H^+$ structures **2** (e.g., **2a** in Figure 2).[79] As the photon energy of 43 kJ/mol is well below the binding energy of **2** (D_0 ≈ 150 kJ/mol),[64,66] only internally excited ions are detected under the employed single-photon absorption conditions,[83−85] giving rise to the large width of D (94 cm^{-1}).

Similar to $EtOH_2^+$−L_n, the $(EtOH)_2H^+$−L_n spectra demonstrate that the most stable intermolecular bonds in **2**−L_n are H-bonds of L to terminal OH donor groups of **2**. Complexation with a single ligand L induces a switch from the (nearly) symmetric EtOH−H^+−HOEt core to a rather asymmetric

$EtOH_2^+$−EtOH core (e.g., **2a**−N_2 in Figure 2).[79] As compared to $\nu_{OH,s/as}$ of **2**, the $\nu_{OH,b}$ mode (band A) of **2**−L is shifted to lower frequency by $\Delta\nu_{OH} = -54$ (Ar) and −135 (N_2) cm^{-1}, in good agreement with the shifts predicted for **2a**−L, $\Delta\nu_{OH} = -44$ (Ar) and −142 (N_2) cm^{-1}. In contrast, the free O−H stretch vibration of **2**−L (band B) is close to $\nu_{OH,s/as}$ of **2** (band D), $\nu_{OH,f} = 3625$ (Ar) and 3633 (N_2) cm^{-1}.

Subsequent solvation of H-bound **2**−L with a second H-bound ligand restores a symmetric microsolvation environment for **2** within **2**−L_2, resulting in a symmetric EtOH−H^+−HOEt core. As a consequence of the weak coupling between the two O−H oscillators engaged in H-bonding with the two ligands, the $\nu_{OH,s}$ and $\nu_{OH,as}$ fundamentals of **2**−$(N_2)_2$ are not resolved (the splitting calculated for **2a**−$(N_2)_2$ amounts to 10 cm^{-1}) and appear as a single band (D) in the $(EtOH)_2H^+$−$(N_2)_2$ spectrum. The observed shifts of band D of **2**−$(N_2)_2$ from bands A and B of **2**−N_2, +34 and −109 cm^{-1}, are consistent with the shifts predicted for **2a**−$(N_2)_2$, +53 and −95 cm^{-1}. The observation of a single band in the O−H stretch range demonstrates that both terminal O−H groups have similar bond strengths. This observation is only compatible with a (nearly) symmetric O−H^+−O proton bridge (Zundel-type structure). If the $(EtOH)_2H^+$−$(N_2)_2$ cluster were to have an asymmetric proton bridge (Eigen-type structure), then both EtOH molecules in the cluster would be very different, i.e., $EtOH_2^+$−OHEt−$(N_2)_2$. One terminal O−H donor bond would then be similar to the O−H bond of neutral EtOH, whereas the other one would be similar to the O−H bonds of $EtOH_2^+$. As these two O−H donor bonds have significantly different acidities, the strengths of the H-bonds to the corresponding N_2 ligands in $EtOH_2^+$−OHEt−$(N_2)_2$ would be rather different, leading to largely separated O−H stretch bands, in contrast to the experimental observation.

Peak D is easily identified also in the spectra of larger $(EtOH)_2H^+$−$(N_2)_n$ clusters with $n > 2$. The lack of absorptions other than D in the O−H stretch range is again taken as evidence for the detection of Zundel-type **2**−$(N_2)_n$ structures in the size range $n = 2-5$, featuring a nearly symmetric O−H^+−O proton bridge. In contrast to H-bonding to OH donor groups, other N_2 binding sites only marginally perturb the Zundel-type EtOH−H^+−HOEt core. Nevertheless, the small incremental blue shifts for $\nu_{OH,s/as}$ of **2**−$(N_2)_n$ ($\Delta\nu_{OH,s/as} = 5-8$ cm^{-1} for $n = 2\rightarrow5$) indicate a stabilization of the (nearly) equivalent terminal O−H bonds upon sequential N_2 microsolvation. Similar to $EtOH_2^+$−L_n, this observation is attributed to noncooperative induction forces.

In general, the complexation-induced shifts caused by the weak intermolecular bonds with L are much smaller for $(EtOH)_2H$−L_n than for $EtOH_2^+$−L_n, consistent with the weaker intermolecular bonds in the former clusters and the smaller acidity of the free O−H bonds of **2** as compared to those of **1** (section 3.1).

3.2.3. $(EtOH)_3H^+$−$(N_2)_n$ Clusters. The IRPD spectra of $(EtOH)_3H^+$−$(N_2)_n$ are compared in Figure 7. The spectrum of bare $(EtOH)_3H^+$ is recorded in the EtOH loss channel (eq 3b), whereas the $(EtOH)_3H^+$−$(N_2)_n$ spectra are obtained in the $(EtOH)_{3/4}H^+$−$(N_2)_m$ fragment channels, indicated as $n \rightarrow m$ (eq 3a). The positions, widths, and assignments of the transitions observed are listed in Table 4. Peak D at 3639 cm^{-1} in the $(EtOH)_3H^+$ spectrum is assigned to the two overlapping free ν_{OH} vibrations of internally excited chain structures such as **3a** (Figure 2), in agreement with the calculated values of 3621 and 3631 cm^{-1} (Table 1). Similar to **2**, also for **3** the photon energy of 44 kJ/mol is well below the energy required to eliminate

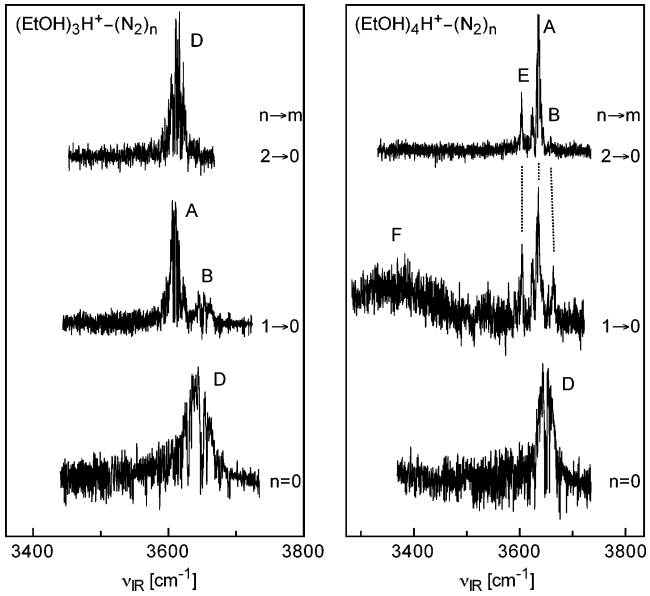

Figure 7. IRPD spectra of $(EtOH)_qH^+$−$(N_2)_n$ recorded in the $(EtOH)_qH^+$−$(N_2)_m$ fragment channel for $q = 3$ and 4, indicated as $n \rightarrow m$ (eq 3a). The $(EtOH)_{3/4}H^+$ spectra are obtained in the EtOH loss channel (eq 3b). The observed transitions are assigned in Table 4. Corresponding transitions are connected by dotted lines.

EtOH ($D_0 \approx 90$ kJ/mol).[64,66] However, as less internal excitation is required for LID of **3** as compared to **2** (46 vs 107 kJ/mol), peak D is narrower for $(EtOH)_3H^+$ than for $(EtOH)_2H^+$ (fwhm = 34 vs 94 cm^{-1}) due to colder spectra.

Band A at 3609 cm^{-1} in the $(EtOH)_3H^+$−N_2 spectrum is attributed to $\nu_{OH,b}$ of **3**−N_2. Its red shift from ν_{OH} of **3** is a clear spectroscopic signature of the intermolecular H-bond of N_2 to one of the two terminal O−H bonds of **3**. The $\nu_{OH,f}$ vibration of **3**−N_2 is identified at 3652 cm^{-1} (B), which is closer to ν_{OH} of **3** (3639 cm^{-1}). These assignments are consistent, with respect to both frequencies and relative IR intensities, with the corresponding ν_{OH} modes calculated for **3a**−N_2 (Table 3).

The lack of detection of free O−H stretch modes in the $(EtOH)_3H^+$−$(N_2)_2$ spectrum confirms that intermolecular H-bonds of N_2 to **3** are significantly more stable than any other binding motif. Moreover, this result demonstrates that the $(EtOH)_3H^+$ isomers observed have only two free O−H bonds available. The appearance of a single narrow band at 3613 cm^{-1} (D) implies that the coupling between the two (nearly) equivalent N_2 solvated O−H oscillators in **3**−$(N_2)_2$ is small. This conclusion is supported by the theoretical splitting of only 1 cm^{-1} predicted for **3a**−$(N_2)_2$.

Comparison of the **3**−$(N_2)_n$ bands with the corresponding transitions of **2**−$(N_2)_n$ reveals that the terminal O−H bonds of **3** are considerably less acidic than those of **2**. For example, $\nu_{OH,b}$ of **3**−N_2 is much higher in frequency than $\nu_{OH,b}$ of **2**−N_2 (3609 vs 3490 cm^{-1}). N_2 solvated O−H stretch bands arising from Zundel-type **3**−$(N_2)_n$ structures are expected to occur in the range of the corresponding **2**−$(N_2)_n$ transitions (3450−3550 cm^{-1}). As the $(EtOH)_3H^+$−$(N_2)_n$ spectra do not feature any resonance below 3580 cm^{-1}, the most stable **3**−$(N_2)_n$ conformers are concluded to be composed of a central $EtOH_2^+$ ion core, solvated by two EtOH and n N_2 ligands ($n \leq 2$). This view is in accord with the calculated **3a**−$(N_2)_{0-2}$ structures. In particular, both the spectra and the calculations reveal that the excess proton is localized on the central EtOH molecule of **3** and not on one of the terminal EtOH units.

3.2.4. $(EtOH)_4H^+$−$(N_2)_n$ Clusters. The IRPD spectra of $(EtOH)_4H^+$−$(N_2)_n$ are compared in Figure 7. The $(EtOH)_4H^+$

spectrum is monitored in the EtOH loss channel (eq 3b), whereas the $(EtOH)_4H^+-(N_2)_n$ spectra are obtained in the $(EtOH)_4H^+-(N_2)_m$ channels, indicated as $n \rightarrow m$ (eq 3a). The positions, widths, and assignments of the transitions observed are listed in Table 4. In contrast to $(EtOH)_qH^+-(N_2)_n$ with $q \leq 3$, the interpretation of the $(EtOH)_4H^+-(N_2)_n$ spectra is less certain. The single peak D at 3649 cm^{-1} in the $(EtOH)_4H^+$ spectrum is assigned to the two overlapping free ν_{OH} vibrations of internally excited H-bonded chain structures, such as **4a** in Figure 2. This band is blue shifted by 10 cm^{-1} from ν_{OH} of $(EtOH)_3H^+$, consistent with weaker and longer terminal O−H bonds in **3**. On the other hand, calculations for **3a** and **4a** yield more similar $\nu_{OH,av}$ and R_{OH} values for these bonds. This slight discrepancy may indicate that either the employed theoretical level is insufficient for the prediction of vibrational frequencies in these H-bonded chains or that the properties of the most stable $(EtOH)_4H^+$ conformer detected in the experiment (**4**) are somewhat different from those calculated for **4a**. Although the detection of a single transition with a symmetric band profile strongly suggests the presence of a symmetric chain structure with a Zundel-type central core, the relatively large width of D (30 cm^{-1}) does not allow for unambiguous structural conclusions.

The $(EtOH)_4H^+-N_2$ spectrum displays three sharp bands, denoted A, B, and E. The detection of more than two transitions points toward the contribution of different isomeric $(EtOH)_4H^+-N_2$ clusters. On the basis of its high intensity, band A at 3632 cm^{-1} is attributed to $\nu_{OH,b}$ of the preferred **4**−N_2 cluster denoted isomer I, in which N_2 binds to one of the two free O−H donor groups of **4**. In line with the smaller acidity of **4** as compared to **3**, the complexation-induced red shift of ν_{OH} is smaller for **4**−N_2 than for **3**−N_2 ($\Delta\nu_{OH} = -17$ vs -30 cm^{-1}). The less intense band E is tentatively assigned to $\nu_{OH,b}$ of a second, less stable **4**−N_2 isomer (II). In contrast to A, band E at 3604 cm^{-1} occurs very close to $\nu_{OH,b}$ of **3**−N_2 (3609 cm^{-1}) suggesting that, similar to the most stable **3**−N_2 structures, isomer II of **4**−N_2 may be composed of a **3**−N_2 core complexed with an additional weakly bound EtOH ligand, i.e., **3**−N_2−EtOH. The latter ligand may, for example, be only weakly van der Waals bonded to **3**−N_2 rather than H-bonded. Finally, band B is attributed to $\nu_{OH,f}$ of both **4**−N_2 isomers. The substantial blue shift of B from D, 13 cm^{-1}, is the same as the shift detected for **3**−N_2, implying a similar stabilizing effect of the free OH group at one end of the H-bonded chain upon N_2 complexation at the OH group at the other end.

In addition to A, B, and E, the $(EtOH)_4H^+-N_2$ spectrum features the onset of a broad band below 3500 cm^{-1} (F). At present, the interpretation of this band is less clear. One possibility may be an assignment to an $(EtOH)_4H^+-N_2$ isomer possessing a neutral $(EtOH)_2$ unit. The bound O−H stretch modes of bare $(EtOH)_2$ isomers occur near 3540 cm^{-1}.[115] Cooperative effects, induced by the presence of the nearby positive charge,[85,114] strengthen the H-bond of a $(EtOH)_2$ unit within a $(EtOH)_4H^+-N_2$ cluster giving rise to additional red shifts.

The $(EtOH)_4H^+-(N_2)_2$ spectrum provides further support for the assignments given for the bands A, B, and E. As compared to $(EtOH)_4H^+-N_2$, the intensity ratio of B and A decreases dramatically (2:5 vs 1:9), indicating that the second N_2 ligand in the most abundant **4**−$(N_2)_2$ isomer (I) binds to free O−H bond of **4**−N_2, forming a (nearly) symmetrically solvated conformer. Consequently, A is attributed to the two overlapping N_2 solvated ν_{OH} modes of a Zundel-type **4**−$(N_2)_2$ structure. Band E is again tentatively assigned to the N_2 solvated O−H stretch of the **3**−$(N_2)_2$−EtOH isomer (II). The very weak detection of B (free O−H stretch) is explained with the minor presence of $(EtOH)_4H^+-(N_2)_2$ isomers with (at least) one free terminal OH group (e.g., isomer II).

4. Further Discussion

Spectroscopic information about $C_2H_7O^+$ isomers in the gas phase is of considerable interest, for example, for the direct identification of these species in various plasma environments. The $EtOH_2^+-L_n$ spectra in Figure 5, combined with the results of quantum chemical calculations, enable the accurate prediction of the O−H stretch frequencies of the bare ethyloxonium ion, $EtOH_2^+$, from the corresponding $EtOH_2^+-L_n$ cluster data. Related studies on H-bound protonated phenol complexes, $C_6H_7O^+-L_n$, showed that the B3LYP/6-311G(2df,2pd) level yields quantitative vibrational O−H stretch frequencies for protonated phenol after the application of an appropriate scaling factor derived from the cluster data.[107] Comparison of the experimental O−H stretch frequencies of $EtOH_2^+-L_{1/2}$ in Table 4 (L = Ar, N_2) with the B3LYP/6-311G(2df,2pd) data results in a scaling factor of 0.9613.[79,116] Applying this factor to the calculated harmonic frequencies of **1a** yields 3511 and 3593 cm^{-1} as best prediction for the experimental values of $\nu_{OH,s}$ and $\nu_{OH,as}$, respectively. These ν_{OH} values are used as experimental reference frequencies for **1** in the discussion below.

To elucidate the substituent-dependent acidity in oxonium ions of protonated aliphatic alcohols (ROH_2^+), it is interesting to compare the properties of the O−H bonds in protonated water (R = H), protonated methanol (R = CH_3), and protonated ethanol (R = C_2H_5). The proton affinity (PA) for protonation at oxygen in ROH increases in the order PA(H_2O) < PA(MeOH) < PA(EtOH) (691 < 754.3 < 776.4 kJ/mol),[117] demonstrating the decreasing acidity for ROH_2^+ along this series. The present B3LYP/6-311G(2df,2pd) calculations fully support this conclusion: $\nu_{OH,av}$ increases (3500 < 3546 < 3552 cm^{-1}) and R_{OH} decreases (0.9793 < 0.9745 < 0.9739 Å) along the series $H_3O^+ \rightarrow MeOH_2^+ \rightarrow EtOH_2^+$. These trends indicate that the properties of the lower part of the intramolecular O−H bond potential ($\nu_{OH,av}$, R_{OH}) can be correlated with the strength of the O−H bonds (PA). Available experimental data for H_3O^+ ($\nu_{OH,av} = 3499$ cm^{-1} and $R_{OH} = 0.974$ Å)[118] compare well with the theoretical results, confirming that the chosen level reliably reproduces the properties of the ROH_2^+ ions. The stronger O−H bonds in ROH_2^+ ions with longer aliphatic chains are rationalized by the more effective delocalization of the positive charge. In general, the incremental effects become smaller as the length of the aliphatic chain increases.

The IR spectra of bare $(EtOH)_{2-4}H^+$ clusters are directly compared in Figure 8a. They are interpreted by H-bonded network chains and do not provide any evidence for the existence of less stable isomers, such as cyclic structures. Similar to $(MeOH)_qH^+$ clusters with $q \geq 5$,[36] cyclic $(EtOH)_qH^+$ structures are supposed to display sharp bands between 3400 and 3500 cm^{-1}, which are clearly absent in the measured IR spectra. The preference for chain isomers in small $(ROH)_qH^+$ clusters may be explained by the high localization of the positive charge. As charge−dipole interactions provide a major contribution to the attraction in these clusters, they prefer roughly linear $O-H^{(+)}-O$ H-bonds resulting in chain-type geometries. The steric constraints required to form small cyclic geometries prevent optimal charge−dipole orientations and suppress the generation of these less favorable isomers in the plasma expansion. The drastic effect of the excess positive charge on the intermolecular interaction is also reflected by the very

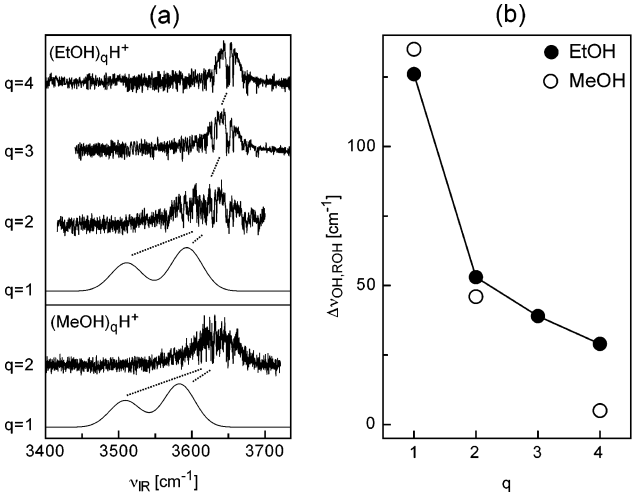

Figure 8. (a) Experimental and theoretical IR spectra of $(MeOH)_qH^+$ and $(EtOH)_qH^+$. The $EtOH_2^+$ and $MeOH_2^+$ spectra are simulations using the scaled (0.9613) vibrational frequencies and IR intensities obtained at the B3LYP/6-311G(2df,2pd) level and a convolution width of 50 cm^{-1}. (b) Red shifts of the ν_{OH} frequencies of the two terminal O−H bonds in $(EtOH)_qH^+$ and $(MeOH)_qH^+$ relative to the corresponding ν_{OH} fundamental of the most stable ROH species. For $q = 1$, the averaged shifts are used. The data point for $(MeOH)_4H^+$ is taken from ref 36.

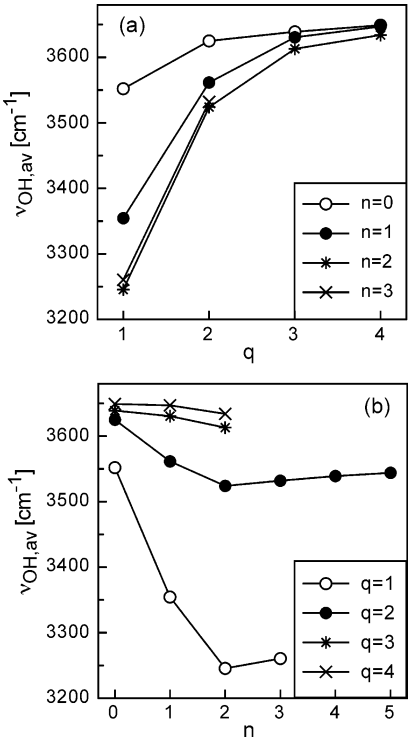

Figure 9. Plots of the average O−H stretching frequencies of the terminal O−H bonds in $(EtOH)_qH^+-(N_2)_n$ as a function of the length of the EtOH chain (a) and the number of weakly bound N_2 ligands (b).

different interaction energies of $(EtOH)_2H^+$, $D_0 \approx 150$ kJ/mol,[64,66] and neutral $(EtOH)_2$, $D_0 \approx 10$ kJ/mol.[90] In contrast to $(ROH)_qH^+$, cyclic isomers are dominant for neutral $(ROH)_q$ clusters ($q \geq 3$),[115,119] because the attraction in these systems is maximized by the larger number of H-bonds. Thus, protonation has a striking impact on the intermolecular PES of alcohol clusters, including both structure and binding energy.

The present data provide experimental evidence for the most stable $(EtOH)_qH^+$ structures in the size range $1 \leq q \leq 4$. Eigen-type ions are preferred for $q =$ odd and Zundel-type isomers dominate for $q =$ even. The preference for one or the other chain motif is strongly dependent on the position and type of additional solvent molecules, as well as on the isomer conformation. For example, asymmetric solvation of **2** with a single N_2 or Ar ligand induces a switch from a EtOH−H$^+$−HOEt to a $EtOH_2^+$ core, whereas a second ligand restores a symmetric environment leading again to a EtOH−H$^+$−HOEt core. Moreover, the $(EtOH)_4H^+-(N_2)_n$ spectra suggest that the most stable **4**−$(N_2)_2$ Zundel-type structure may coexist with a less stable Eigen-type conformer composed of a **3**−$(N_2)_2$ core, which is complexed by an additional weakly bound EtOH ligand, i.e., **3**−$(N_2)_2$−EtOH. In general, the experimental detection of both Eigen- and Zundel-type ions are in line with the predictions of the quantum chemical calculations. However, it is noted once again that the structures calculated for $(EtOH)_3H^+$ and $(EtOH)_4H^+$, **3a** and **4a**, are possibly not the most stable conformers (rotamers) of these clusters and may slightly differ from the ones observed experimentally.

Analysis of the ν_{OH} frequencies of the terminal EtOH units in $(EtOH)_qH^+$ demonstrates the change in their acidity as a function of the chain length q (Figure 8). In addition to the $(EtOH)_{2-4}H^+$ spectra, Figure 8a includes the IRPD spectrum of $(MeOH)_2H^+$. To the best of our knowledge, this is the first IR spectrum of this fundamental dimer. Along with the available $(MeOH)_4H^+$ spectrum,[36−38] it allows us to probe important properties of the intra- and intermolecular bonds in $(ROH)_qH^+$ chains as a function of both the cluster size q and the length of the chain R. For this purpose, Figure 8b plots the red shifts of the ν_{OH} frequencies of the two terminal O−H bonds in $(EtOH)_qH^+$ and $(MeOH)_qH^+$ relative to the ν_{OH} fundamentals of isolated EtOH (3678 cm^{-1}) and MeOH (3681 cm^{-1}), $\Delta\nu_{OH,ROH}$, vs the cluster size q. A larger red-shift implies a stronger perturbation of the terminal ROH units by stronger intermolecular bonds to the interior protonated moiety. As a result, their O−H bonds are weaker and more acidic. Inspection of Figure 8b shows that the terminal O−H bonds become stronger and less acidic for increasing cluster size q, leading to smaller $\Delta\nu_{OH,ROH}$. Interestingly, although for $q = 1$ the O−H bonds in $EtOH_2^+$ are weaker than in $MeOH_2^+$, the decrease is less pronounced for $(EtOH)_qH^+$ than for $(MeOH)_qH^+$. Apparently, the substitution of methyl by ethyl groups leads to a significant increase in the strength of the H-bonds along the $(ROH)_qH^+$ chains. A similar effect has also been reported for neutral $(EtOH)_q$ and $(MeOH)_q$ clusters.[115] Possibly, this observation is of relevance for explaining subtle differences in the proton transfer mechanisms in liquid alcohols via locally protonated H-bonded network chains.[57]

Figure 9 plots $\nu_{OH,av}$ of the terminal O−H bonds in the most stable $(EtOH)_qH^+-(N_2)_n$ isomers vs the cluster size for variable size of both the interior $(EtOH)_qH^+$ network, q (Figure 9a), and the number of the N_2 ligands, n (Figure 9b). As discussed above, for $n = 0$ and increasing q, the terminal O−H bonds become shorter and less acidic, leading to an increase in $\nu_{OH,av}$ along the series **1** > **2** > **3** > **4** (Figure 9a). Interestingly, this effect is enhanced for successive solvation of the two available terminal O−H bonds in $(EtOH)_qH^+$ by one or two weakly bound N_2 ligands ($n = 1, 2$). As these H-bound N_2 ligands cause the O−H bonds in $(EtOH)_qH^+-(N_2)_{1/2}$ to become weaker, the N_2 solvated OH groups provide a more sensitive indicator for the acidity of the $(EtOH)_qH^+$ chain, because they lead to larger q-dependent $\nu_{OH,av}$ shifts for $(EtOH)_qH^+-(N_2)_{1/2}$ as compared to bare $(EtOH)_qH^+$ ($n = 0$). The same trends as derived from Figure 9a are also evident in Figure 9b. For a given q, $\nu_{OH,av}$ experiences substantial incremental red shift for $n \leq 2$ arising from the H-bonds of the first two N_2 ligands to the two available terminal O−H bonds of $(EtOH)_qH^+$. In line with the decreasing

acidity along the series **1** > **2** > **3** > **4**, however, the H-bonds to N_2 become weaker and the red shifts decrease. For example, the total red shifts for $n = 2$ are 8.6% for $EtOH_2^+$, 2.8% for $(EtOH)_2H^+$, 0.7% for $(EtOH)_3H^+$, and 0.4% for $(EtOH)_4H^+$. The preferred binding sites of further N_2 ligands in $(EtOH)_qH^+-(N_2)_n$ with $n > 2$ are not obvious and include H-bonding to C−H bonds of the ethyl groups or further solvation of the excess proton. The minor increase of $\nu_{OH,av}$ to higher frequencies for $n > 2$ for a given q in Figure 9 is typical for noncooperative induction forces. Solvation of the $(EtOH)_qH^+-(N_2)_2$ cluster ions with additional N_2 ligands weakens the H-bonds to the first two N_2 ligands, thereby strengthening the terminal O−H bonds. The closure of the first solvation subshell for $n = 2$ confirms the detection of $(EtOH)_qH^+-(N_2)_n$ clusters featuring an interior $(EtOH)_qH^+$ chain with one available acidic O−H group at each end.

According to eq 3a, several $(EtOH)_qH^+-L_m$ fragment channels may be observed for a given $(EtOH)_qH^+-L_n$ parent complex with $n > 1$. The number of evaporated ligands L, $n - m$, depends sensitively on the cluster size (n, q), the type of ligand (Ar, N_2), and the excitation frequency. Similar to previous studies on related systems using the same experimental setup,[80,114] the range of observed fragment channels m for a given n is rather narrow. For all $(EtOH)_qH^+-L_n$ clusters considered, only one dominant fragment channel is observed, and this channel carries between 70 and 100% of the total LID signal (e.g., Figure 4). This information can be used to estimate approximate ligand binding energies, assuming a simple statistical model for the evaporation process. The basic assumptions of this model are outlined in refs 91 and 100. The model assumes that all the energy of the absorbed photon can be used for ligand evaporation (only single photon absorption processes are observed). Hence, the photon energy must be larger than the binding energy of the $n - m$ evaporated ligands but smaller than the sum of the dissociation energies of the $n - m + 1$ most weakly bound ligands. Moreover, ligands solvated at (roughly) equivalent positions are assumed to have the same binding energy. For this purpose, the ligands L are classified into H-bound ($n = 1$, 2) and other ligands ($n > 2$), with dissociation energies of $D_0(H) > D_0(o)$, respectively. First, the $EtOH_2^+-L_n$ clusters are considered. The $EtOH_2^+-Ar_n$ ($n \leq 2$) clusters evaporate all ligands upon excitation with $\nu_{IR} > 3300$ cm^{-1}. This observation results in $D_0(H) < 1700$ cm^{-1}, consistent with the calculated values, $D_e(H) \sim 800$ cm^{-1} (Table 2). For the $EtOH_2^+-(N_2)_n$ clusters, the photofragmentation data suggest $D_0(H) = 2400 \pm 800$ cm^{-1} and $D_0(o) < 1600$ cm^{-1}, again in good agreement with the predicted binding energy, $D_e(H) \sim 2700$ cm^{-1}. In general, the binding energies in $(EtOH)_2H^+-L_n$ are much weaker than in $EtOH_2^+-L_n$, because the OH groups in $(EtOH)_2H^+$ are less acidic and the positive charge is distributed over a larger ion core. In particular, for $(EtOH)_2H^+-(N_2)_n$ the fragmentation data suggest $D_0(H) = 1300 \pm 500$ cm^{-1} and $D_0(o) < 1200$ cm^{-1}, in line with the calculated value, $D_e(H) \sim 1600$ cm^{-1}. The fragmentation data for $(EtOH)_qH^+-(N_2)_n$ with $q = 3$ and 4 are less detailed as compared to $q \leq 2$. However, the experimental limits derived, $D_0(H) < 1800$ cm^{-1}, are again compatible with the theoretical values, $D_e(H) \sim 1000$ and 900 cm^{-1} for $q = 3$ and 4, respectively. In general, both the experimental and theoretical binding energies in $(EtOH)_qH^+-L_n$, $D_0(H)$ and $D_e(H)$, drop substantially with increasing chain length q, consistent with the decreasing acidity of the terminal OH groups already deduced from the O−H stretch frequencies (Figure 9).

5. Concluding Remarks

In conclusion, the fruitful combination of IR spectroscopy, mass spectrometry, and quantum chemistry is shown to provide a powerful tool to characterize fundamental properties of size-selected proton wires isolated in the gas phase. IRPD spectra of $(EtOH)_qH^+-L_n$ are interpreted with H-bonded chain structures composed of q EtOH units, n inert ligands L, and an excess proton. Depending on the number, position, and type of solvent molecules, as well as on the isomer conformation, the excess proton in $(EtOH)_qH^+$ is either strongly localized on one or (nearly) equally shared between two EtOH molecules, resulting in Eigen-type or Zundel-type structural motifs. According to the IR spectra, the most stable $(EtOH)_qH^+$ geometries correspond to Eigen-type structures for $q = 1$ and 3 and Zundel-type structures for $q = 2$ and 4. In the case of $(EtOH)_4H^+$, minor spectral features are interpreted with the detection of less stable Eigen-type conformers, suggesting that the strict even/odd alternation becomes less pronounced for longer chains. The acidity of the two terminal OH groups in the $(EtOH)_qH^+$ chains decreases with the length of the chain (q). Comparison between $(ROH)_qH^+$ with R = CH_3 and C_2H_5 shows that the acidity of the terminal O−H groups increases with the length of the aliphatic rest R. In contrast to neutral $(EtOH)_q$ clusters but similar to $(MeOH)_qH^+$ and $(H_2O)_qH^+$ clusters, cyclic $(EtOH)_qH^+$ isomers are not detected in the size range investigated ($q \leq 4$), indicative of the substantial impact of the excess proton on the properties of small aliphatic alcohol networks. The preferred microsolvation motif between $(EtOH)_qH^+$ chains and weakly bound nonpolar ligands L = Ar/N_2 corresponds to H-bonding of the first two ligands to the two available terminal OH groups of $(EtOH)_qH^+$. Subsequently, less favorable binding sites are occupied. Asymmetric solvation of $(EtOH)_qH^+$ with Zundel-type ion cores ($q = 2$, 4) induces a switch toward Eigen-type structures. Similar effects have also been reported for solvation of $(H_2O)_qH^+$ with weakly bound ligands.[18,28] As the chain length of $(EtOH)_qH^+$ increases, the terminal O−H bonds become shorter and less acidic so that, for example, in $(EtOH)_4H^+-N_2$ other ligand binding sites become competitive with H-bonding. In general, the $(EtOH)_qH^+-L_n$ data illustrate the high sensitivity of IR spectroscopy for probing the acidity of cluster ions. The weakly bound ligands enable cluster dissociation under single-photon absorption conditions, lead to the detection of narrow bands of cold cluster species, and drastically enhance the effects of the length of the $(EtOH)_qH^+$ chain on the acidity of their terminal OH groups. Similarly to $(H_2O)_2H^+$,[14,24] $(EtOH)_qH^+$ clusters will be ideal targets for IR multiphoton dissociation (IRMPD) studies in the frequency range below 2500 cm^{-1} using high power free electron lasers, to directly probe the vibrational motions of the excess proton in $(EtOH)_qH^+$ proton wires.

Acknowledgment. This study was supported by the Deutsche Forschungsgemeinschaft (DO 729/2-2) and the Fonds der Chemischen Industrie. O.D. is supported via a Heisenberg Fellowship (DO 729/1-2).

References and Notes

(1) Eigen, M. *Angew. Chem., Int. Ed. Engl.* **1964**, *3*, 1.
(2) Schuster, P.; Zundel, G.; Sandorfy, C. *The Hydrogen Bond-Recent Developments in Theory and Experiments*; North-Holland: Amsterdam, 1976; Vols. 1−3.
(3) Agmon, N. *Chem. Phys. Lett.* **1995**, *244*, 456.
(4) Marx, D.; Tuckerman, M. E.; Hutter, J.; Parrinello, M. *Nature (London)* **1999**, *397*, 601.
(5) Cowin, J. P.; Tsekouras, A. A.; Iedema, M. J.; Wu, K.; Ellison, G. B. *Nature (London)* **1999**, *398*, 405.
(6) Hynes, J. T. *Nature (London)* **1999**, *397*, 565.

(7) Tuckerman, M. E.; Marx, D.; Klein, M. L.; Parrinello, M. *Science* **1997**, *275*, 817.
(8) Rousseau, R.; Kleinschmidt, V.; Schmitt, U. W.; Marx, D. *Phys. Chem. Chem. Phys.* **2004**, *6*, 1848.
(9) Stryer, L. *Biochemistry*; Freeman: New York, 1996.
(10) Jeffrey, G. A.; Saenger, W. *Hydrogen Bonding in Biological Systems*; Springer: Heidelberg, Germany, 1991.
(11) Kreuer, K. D. *Solid State Ionics* **1997**, *94*, 55.
(12) Kreuer, K. D. *Solid State Ionics* **2000**, *136*−*137*, 149.
(13) Niedner-Schatteburg, G.; Bondybey, V. E. *Chem. Rev.* **2000**, *100*, 4059.
(14) Asmis, K. R.; Pivonka, N. L.; Santambrogio, G.; Brümmer, M.; Kaposta, C.; Neumark, D. M.; Wöste, L. *Science* **2003**, *299*, 1375.
(15) Kim, J.; Schmitt, U. W.; Gruetzmacher, J. A.; Voth, G. A.; Scherer, N. E. *J. Chem. Phys.* **2002**, *116*, 737.
(16) Huneycutt, A.; Saykally, R. *Science* **2003**, *299*, 1329.
(17) Bieske, E. J.; Dopfer, O. *Chem. Rev.* **2000**, *100*, 3963.
(18) Okumura, M.; Yeh, L. I.; Myers, J. D.; Lee, Y. T. *J. Phys. Chem.* **1990**, *94*, 3416.
(19) Duncan, M. *Int. J. Mass Spectrom.* **2000**, *200*, 545.
(20) Bakker, J. M.; Satink, R. G.; von Helden, G.; Meijer, G. *Phys. Chem. Chem. Phys.* **2002**, *4*, 24.
(21) Fujii, A.; Fujimaki, E.; Ebata, T.; Mikami, N. *J. Chem. Phys.* **2000**, *112*, 6275.
(22) Robertson, W. H.; Johnson, M. A. *Annu. Rev. Phys. Chem.* **2003**, *54*, 173.
(23) Duncan, M. A. *Int. Rev. Phys. Chem.* **2003**, *22*, 407.
(24) Fridgen, T. D.; McMahon, T. B.; MacAleese, L.; Lemaire, J.; Maitre, P. *J. Phys. Chem. A* **2004**, *108*, 9008.
(25) Schwarz, H. A. *J. Chem. Phys.* **1977**, *67*, 5525.
(26) Linnartz, H.; Verdes, D.; Speck, T. *Rev. Sci. Instrum.* **2000**, *71*, 1811.
(27) Okumura, M.; Yeh, L. I.; Myers, J. D.; Lee, Y. T. *J. Chem. Phys.* **1986**, *85*, 2328.
(28) Yeh, L. I.; Okumura, M.; Myers, J. D.; Price, J. M.; Lee, Y. T. *J. Chem. Phys.* **1989**, *91*, 7319.
(29) Yeh, L. I.; Lee, Y. T.; Hougen, J. T. *J. Mol. Spectrosc.* **1994**, *164*, 473.
(30) Jiang, J. C.; Wang, Y. S.; Chang, H. C.; Lin, S. H.; Lee, Y. T.; Niedner-Schattenburg, G.; Chang, H. C. *J. Am. Chem. Soc.* **2000**, *122*, 1398.
(31) Shin, J. W.; Hammer, N. I.; Diken, E. G.; Johnson, M. A.; Walters, R. S.; Jaeger, T. D.; Duncan, M. A.; Christie, R. A.; Jordan, K. D. *Science* **2004**, *304*, 1137.
(32) Miyazaki, M.; Fujii, A.; Ebata, T.; Mikami, N. *Science* **2004**, *304*, 1134.
(33) Headrick, J. M.; Bopp, J. C.; Johnson, M. A. *J. Chem. Phys.* **2004**, *121*, 11523.
(34) Wu, C.-C.; Lin, C.-K.; Chang, H.-C.; Jiang, J.-C.; Kuo, J.-L.; Klein, M. L. *J. Chem. Phys.* **2005**, *122*, 074315.
(35) Wang, Y.-S.; Tsai, C.-H.; Lee, Y. T.; Chang, H. C.; Jiang, J. C.; Asvany, O.; Schlemmer, S.; Gerlich, D. *J. Phys. Chem. A* **2003**, *107*, 4217.
(36) Chang, H. C.; Jiang, J. C.; Lin, S. H.; Lee, Y. T.; Chang, H. C. *J. Phys. Chem. A* **1999**, *103*, 2941.
(37) Wu, C. C.; Chaudhuri, C.; Jiang, J. C.; Lee, Y. T.; Chang, H. C. *J. Phys. Chem. A* **2004**, *108*, 2859.
(38) Fujii, A.; Enomoto, S.; Miyazaki, M.; Mikami, N. *J. Phys. Chem. A* **2005**, *109*, 138.
(39) Wu, C. C.; Jiang, J. C.; Boo, D. W.; Lin, S. H.; Lee, Y. T.; Chang, H. C. *J. Chem. Phys.* **2000**, *112*, 176.
(40) Chaudhuri, C.; Jiang, J. C.; Wang, X.; Lee, Y. T.; Chang, H. C. *J. Chem. Phys.* **2000**, *112*, 7279.
(41) Jiang, J. C.; Chaudhuri, C.; Lee, Y. T.; Chang, H. C. *J. Phys. Chem. A* **2002**, *106*, 10937.
(42) Wang, Y. S.; Jiang, J. C.; Cheng, C. L.; Lin, S. H.; Lee, Y. T.; Chang, H. C. *J. Chem. Phys.* **1997**, *107*, 9695.
(43) Wang, Y. S.; Chang, H. C.; Jiang, J. C.; Lin, S. H.; Lee, Y. T.; Chang, H. C. *J. Am. Chem. Soc.* **1998**, *120*, 8777.
(44) Chang, H. C.; Wang, Y. S.; Lee, Y. T.; Chang, H. C. *Int. J. Mass Spectrom.* **1998**, *179/180*, 91.
(45) Chang, H. C.; Jiang, J. C.; Hahndorf, I.; Lin, S. H.; Lee, Y. T.; Chang, H. C. *J. Am. Chem. Soc.* **1999**, *121*, 4443.
(46) Hahndorf, I.; Jiang, J. C.; Chang, H. C.; Wu, C. C.; Chang, H. C. *J. Phys. Chem. A* **1999**, *103*, 8753.
(47) Frisch, M. J.; Del Bene, J. E.; Binkley, J. S.; Schaefer, H. F., III. *J. Chem. Phys.* **1986**, *84*, 2279.
(48) Lee, E. P. F.; Dyke, J. M.; Michl, J. *Mol. Phys.* **1991**, *73*, 375.
(49) Xie, Y.; Remington, R. B.; Schaefer, H. F. *J. Chem. Phys.* **1994**, *101*, 4878.
(50) Ojamäe, L.; Shavitt, I.; Singer, S. J. *Int. J. Quantum Chem.* **1995**, *Suppl. 29*, 657.
(51) Klein, S.; Kochanski, E.; Strich, A.; Sadlej, A. J. *J. Phys. Chem. A* **1997**, *101*, 4799.
(52) Valeev, E. F.; Schaefer, H. F., III. *J. Chem. Phys.* **1998**, *108*, 7197.
(53) Wales, D. J. *J. Chem. Phys.* **1999**, *110*, 10403.
(54) Auer, A. A.; Helgaker, T.; Klopper, W. *Phys. Chem. Chem. Phys.* **2000**, *2*, 2235.
(55) McCoy, A.; Huang, X.; Carter, S.; Landeweer, M. Y.; Bowman, J. M. *J. Chem. Phys.* **2005**, *122*, 061101.
(56) Huang, X.; Braams, B. J.; Bowman, J. M. *J. Chem. Phys.* **2005**, *122*, 044308.
(57) Morrone, J. A.; Tuckerman, M. E. *J. Chem. Phys.* **2002**, *117*, 4403.
(58) Jarvis, V. M.; Villanueva, M. A.; Bostwick, D. E.; Moran, T. F. *Org. Mass Spectrom.* **1993**, *28*, 595.
(59) Fairley, D. A.; Scott, G. B. I.; Freeman, C. G.; MacIagan, R. G. A. R.; McEwan, M. J. *J. Phys. Chem. A* **1997**, *101*, 2848.
(60) Matthews, K. K.; Adams, N. G.; Fisher, N. D. *J. Phys. Chem. A* **1997**, *101*, 2841.
(61) Mason, R. S.; Naylor, J. C. *J. Phys. Chem. A* **1998**, *102*, 10090.
(62) Sirois, M.; George, M.; Holmes, J. L. *Org. Mass. Spectrom.* **1994**, *29*, 11.
(63) Jarrold, M. F.; Kirchner, N. J.; Liu, S.; Bowers, M. T. *J. Phys. Chem.* **1986**, *90*, 78.
(64) Mair, C.; Lezius, M.; Herman, Z.; Märk, T. D. *J. Chem. Phys.* **2003**, *118*, 7090.
(65) Bouchoux, G.; Hoppilliard, Y. *J. Am. Chem. Soc.* **1990**, *112*, 9110.
(66) Mair, C.; Fedor, J.; Lezius, M.; Scheier, P.; Probst, M.; Herman, Z.; Märk, T. D. *New J. Phys.* **2003**, *5*, 9.
(67) Fridgen, T. D.; McMahon, T. B. *J. Phys. Chem. A* **2002**, *106*, 9648.
(68) McCormack, J. A. D.; Mayer, P. M. *Int. J. Mass Spectrom.* **2001**, *207*, 183.
(69) Feng, W. Y.; Lifshitz, C. *Int. J. Mass Spectrom. Ion Proc.* **1995**, *149/150*, 13.
(70) Bomse, D. S.; Bouchoux, G. *J. Am. Chem. Soc.* **1981**, *103*, 3292.
(71) Shukla, A. K.; Stace, A. J. *J. Phys. Chem.* **1988**, *92*, 2579.
(72) Mafuné, F.; Kohno, J.; Kondow, T. *J. Phys. Chem.* **1996**, *100*, 10041.
(73) Pearson, J. C.; Sastry, K. V. L. N.; Herbst, E.; De Lucia, F. *Astrophys. J.* **2002**, *480*, 420.
(74) Charnley, S. B.; Kress, M. E.; Tielens, A. G. G. M.; Millar, T. J. *Astrophys. J.* **1995**, *448*, 232.
(75) Herbst, E. *Astrophys. J.* **1987**, *313*, 867.
(76) Swanton, D. J.; Marsden, D. C. J.; Darom, L. *Org. Mass Spectrom.* **1991**, *26*, 227.
(77) Jursic, B. S. *J. Mol. Struct. (THEOCHEM)* **1999**, *487*, 163.
(78) Audier, H. E.; Koyanagi, G. K.; McMahon, T. B.; Tholmann, D. *J. Phys. Chem.* **1996**, *100*, 8220.
(79) Solcà, N.; Dopfer, O. *J. Am. Chem. Soc.* **2004**, *126*, 9520.
(80) Dopfer, O. *Int. Rev. Phys. Chem.* **2003**, *22*, 437.
(81) Solcà, N.; Dopfer, O. *Chem. Phys. Lett.* **2001**, *342*, 191.
(82) Linstrom, P. J.; Mallard, W. G. *NIST Chemistry WebBook*; NIST Standards and Technology, Gaithersburg MD (http://webbook.nist.gov), 2001.
(83) Solcà, N.; Dopfer, O. *J. Am. Chem. Soc.* **2003**, *125*, 1421.
(84) Solcà, N.; Dopfer, O. *J. Chem. Phys.* **2004**, *121*, 769.
(85) Solcà, N.; Dopfer, O. *J. Phys. Chem. A* **2003**, *107*, 4046.
(86) Guelachvili, G.; Rao, K. N. *Handbook of Infrared Standards*; Academic Press: London, 1993.
(87) Camy-Peyret, C.; Flaud, J. M.; Guelachvili, G.; Amiot, C. *Mol. Phys.* **1973**, *26*, 825.
(88) Frisch, M. J.; et al. *Gaussian 98*, Revision A.7; Gaussian, Inc.: Pittsburgh, PA, 1998.
(89) Boys, S. F.; Bernardi, F. *Mol. Phys.* **1970**, *19*, 553.
(90) Dyczmons, V. *J. Phys. Chem. A* **2004**, *108*, 2080.
(91) Nizkorodov, S. A.; Dopfer, O.; Ruchti, T.; Meuwly, M.; Maier, J. P.; Bieske, E. J. *J. Phys. Chem.* **1995**, *99*, 17118.
(92) Nizkorodov, S. A.; Roth, D.; Olkhov, R. V.; Maier, J. P.; Dopfer, O. *Chem. Phys. Lett.* **1997**, *278*, 26.
(93) Dopfer, O.; Nizkorodov, S. A.; Meuwly, M.; Bieske, E. J.; Maier, J. P. *Int. J. Mass Spectrom. Ion Proc.* **1997**, *167/168*, 637.
(94) Dopfer, O.; Nizkorodov, S. A.; Olkhov, R. V.; Maier, J. P.; Harada, K. *J. Phys. Chem. A* **1998**, *102*, 10017.
(95) Olkhov, R. V.; Nizkorodov, S. A.; Dopfer, O. *J. Chem. Phys.* **1998**, *108*, 10046.
(96) Olkhov, R. V.; Nizkorodov, S. A.; Dopfer, O. *Chem. Phys.* **1998**, *239*, 393.
(97) Olkhov, R. V.; Dopfer, O. *Chem. Phys. Lett.* **1999**, *314*, 215.
(98) Dopfer, O.; Olkhov, R. V.; Maier, J. P. *J. Phys. Chem. A* **1999**, *103*, 2982.
(99) Solcà, N.; Dopfer, O. *Chem. Phys. Lett.* **2000**, *325*, 354.
(100) Solcà, N.; Dopfer, O. *J. Phys. Chem. A* **2001**, *105*, 5637.
(101) Dopfer, O.; Solcà, N.; Olkhov, R. V.; Maier, J. P. *Chem. Phys.* **2002**, *283*, 85.
(102) Dopfer, O.; Roth, D.; Maier, J. P. *J. Am. Chem. Soc.* **2002**, *124*, 494.
(103) Dopfer, O.; Roth, D.; Maier, J. P. *Int. J. Mass. Spectrosc.* **2002**, *218*, 281.

(104) Solcà, N.; Dopfer, O. *Eur. Phys. J. D* **2002**, *20*, 469.
(105) Solcà, N.; Dopfer, O. *J. Phys. Chem. A* **2002**, *106*, 7261.
(106) Solcà, N.; Dopfer, O. *Chem. Phys. Lett.* **2003**, *369*, 68.
(107) Solcà, N.; Dopfer, O. *J. Am. Chem. Soc.* **2004**, *126*, 1716.
(108) Solcà, N.; Dopfer, O. *J. Chem. Phys.* **2004**, *120*, 10470.
(109) Dopfer, O.; Roth, D.; Maier, J. P. *J. Phys. Chem. A* **2000**, *104*, 11702.
(110) Dopfer, O. *J. Phys. Chem. A* **2000**, *104*, 11693.
(111) Andrei, H. S.; Solcà, N.; Dopfer, O. *J. Phys. Chem. A* **2005**, *109*, 3598.
(112) Andrei, H. S.; Solcà, N.; Dopfer, O. *Phys. Chem. Chem. Phys.* **2004**, *6*, 3801.
(113) Solcà, N.; Dopfer, O. *Phys. Chem. Chem. Phys.* **2004**, *6*, 2732.
(114) Dopfer, O. *Z. Phys. Chem.* **2005**, *219*, 125.
(115) Provencal, R. A.; Paul, J. B.; Roth, K.; Chapo, C.; Casaes, R. N.; Saykally, R. J.; Tschumper, G. S.; Schaefer, H. F., III. *J. Chem. Phys.* **1999**, *110*, 4258.
(116) The harmonic B3LYP/6-311G(2df,2pd) frequencies of the two terminal O−H stretch modes used to determine the scaling factor are 3483.3 and 3707.9 cm^{-1} (**1a**−Ar(*a*)), 3286.1 and 3716.1 cm^{-1} (**1a**−N_2(*a*)), 3497.3 and 3546.4 cm^{-1} (**1a**−Ar_2), and 3373.9 and 3398.3 cm^{-1} (**1a**−$(N_2)_2$).
(117) Hunter, E. P. L.; Lias, S. G. *J. Phys. Chem. Ref. Data* **1998**, *27*, 413.
(118) Tang, J.; Oka, T. *J. Mol. Spectrosc.* **1999**, *196*, 120.
(119) Buck, U.; Huisken, F. *Chem. Rev.* **2000**, *100*, 3863.